

Explicit stabilized multirate method for stiff differential equations

Assyr Abdulle*, Marcus J. Grote†, Giacomo Rosilho de Souza*

Abstract

Stabilized Runge–Kutta methods are especially efficient for the numerical solution of large systems of stiff nonlinear differential equations because they are fully explicit. For semi-discrete parabolic problems, for instance, stabilized Runge–Kutta methods overcome the stringent stability condition of standard methods without sacrificing explicitness. However, when stiffness is only induced by a few components, as in the presence of spatially local mesh refinement, their efficiency deteriorates. To remove the crippling effect of a few severely stiff components on the entire system of differential equations, we derive a modified equation, whose stiffness solely depend on the remaining mildly stiff components. By applying stabilized Runge–Kutta methods to this modified equation, we then devise an explicit multirate Runge–Kutta–Chebyshev (mRKC) method whose stability conditions are independent of a few severely stiff components. Stability of the mRKC method is proved for a model problem, whereas its efficiency and usefulness are demonstrated through a series of numerical experiments.

Key words. stabilized Runge–Kutta methods, explicit time integrators, stiff equations, multirate methods, local time-stepping, parabolic problems, Chebyshev methods.

AMS subject classifications. 65L04, 65L06, 65L20.

1 Introduction

We consider the system of stiff (nonlinear) differential equations,

$$y' = f(y) := f_F(y) + f_S(y), \quad y(0) = y_0, \quad (1.1)$$

where $f : \mathbb{R}^n \rightarrow \mathbb{R}^n$ splits into an expensive but only mildly stiff part, f_S , associated with relatively slow (S) time-scales, and a cheap but severely stiff part, f_F , associated with fast (F) time-scales. Typical applications include chemical reactions and electrical circuits with disparate time-scales, but also spatial discretizations of diffusion dominated (parabolic) partial differential equations (PDEs) with local mesh refinement. Semi-discrete parabolic PDEs, in particular, lead to large systems of stiff ordinary differential equations, where the eigenvalues of the Jacobian matrix, $\partial f / \partial y$, lie in a narrow strip along the negative real axis whose extent scales as H^{-2} for a mesh size H . In the presence of local mesh refinement, f_S, f_F in (1.1) then correspond to discrete diffusion operators in the coarse and locally refined region of the mesh, respectively. Although f_F involves only a small number of degrees of freedom, the extreme eigenvalue of its Jacobian will determine the spectral radius ρ of $\partial f / \partial y$.

In contrast to multiscale methods [3, 12, 13, 60], *we do not assume any scale separation* in (1.1); hence, f_F may contain *both fast and slow* scales. In a situation of local mesh refinement, for instance, when f_S and f_F each represent the discrete Laplacian in the coarse and refined regions, both Jacobians in fact contain small eigenvalues in magnitude; hence, the spectrum of $\partial f / \partial y$ cannot

*ANMC, Institute of Mathematics, École Polytechnique Fédérale de Lausanne, 1015 Lausanne, Switzerland asyr.abdulle@epfl.ch, giacomo.rosilhodesouza@epfl.ch

†Department of Mathematics and Computer Science, University of Basel, Spiegelgasse 1, 4051 Basel, Switzerland marcus.grote@unibas.ch

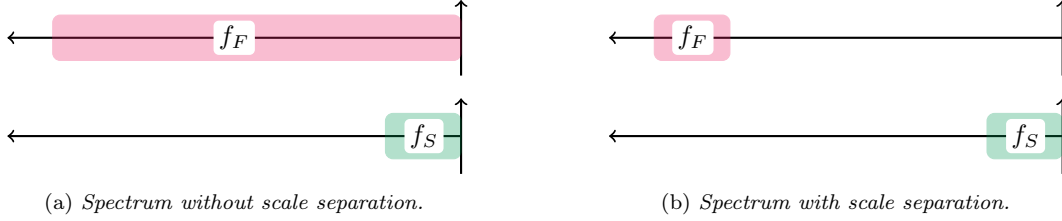


Figure 1. Stiff problems with identical spectral radii but different eigenvalues distribution.

simply be split into fast and slow modes, as in Figure 1(a). This stands in sharp contrast to the underlying assumption of recently introduced multiscale methods for stiff (dissipative) ODEs, such as the heterogeneous multiscale method (HMM) [12, 13] or the projective method [19] which all require scale separation, as in Figure 1(b).

Standard explicit methods are notoriously inefficient for stiff differential equations due to their stringent stability constraint on the step size, τ , which for parabolic problems must be proportional to H^2 . Implicit methods, on the other hand, are unconditionally stable but require at every time step the solution of an $n \times n$ linear (or possibly nonlinear) system of equations, a high price to pay when n is large. Moreover, when sheer size calls for using iterative methods, the overall performance heavily relies on the availability of efficient preconditioners while the convergence of Newton-like nonlinear iterations is not even guaranteed for larger step sizes.

Stabilized Runge–Kutta (RK) (or Chebyshev) methods fall somewhere between explicit and implicit methods: they are explicit and thus avoid the solution of large systems of equations, while their stability interval on the negative real axis is proportional to s^2 for an s -stage method. Thanks to this remarkable quadratic dependency, the work load (number of stages s) per time step only needs to scale linearly with H^{-1} for parabolic PDEs, in contrast to the quadratic increase in the number of time steps required by standard explicit integrators. Stabilized RK methods are thus particularly efficient for the time integration of large-scale, possibly nonlinear, parabolic PDEs [11]. Several stabilized RK methods have been proposed in the literature, such as DUMKA methods, based on the composition of Euler steps [36, 37, 39], Runge–Kutta–Chebyshev (RKC) methods, based on the linear combination of Chebyshev polynomials [54, 59, 64] and orthogonal Runge–Kutta–Chebyshev methods (ROCK), based on optimal orthogonal stabilized functions [1, 2]; note that ROCK and RKC methods differ only beyond order one. Still, when applied to (1.1), the number of stages s of any standard stabilized RK method will, yet again, be determined by the stiffest part f_F and the method eventually become inefficient.

To overcome the stringent step size restriction due to the cheap but stiffer part, f_F , while retaining the efficiency of explicit time integration for f_S , *multirate methods* use a smaller step size, or even an entirely different scheme, for integrating f_F . Since the early work of Rice [42] and the work of Gear and Wells [20] who proposed a number of multirate strategies for the interlaced time integration of the “fast” and “slow” components using classical multistep schemes, various explicit, implicit or hybrid multirate schemes have been developed based on Runge–Kutta methods using splitting techniques for “fast” and “slow” components or extrapolation techniques [7, 14, 24, 25, 32, 35, 49, 50, 53]. All these methods require a predictor step and either interpolate or extrapolate between “fast” and “slow” state variables, which is prone to instability. Although some of the implicit-explicit (IMEX) methods are provably stable, they are more cumbersome to implement and rapidly become too expensive as the number of “fast” unknowns increases.

More recently, Günther and Sandu exploited the generalized additive Runge–Kutta (GARK) framework [47] to devise multirate GARK (MrGARK) methods [26]. Many explicit, implicit and hybrid schemes are developed (up to fourth order accuracy) in [43, 48], although some degree of implicitness is typically required to achieve a larger stability domain. In [44, 46, 51], multirate infinitesimal step (MIS) methods [34, 65], which assume the fast variables integrated exactly, are recast into the GARK framework and further generalized. The resulting multirate infinitesimal (MRI)-GARK methods extend exponential integrators [31] to the nonlinear case, where again the fast (nonlinear) dynamics are integrated exactly. When these semi-discrete schemes are used in

practice, that is, in a fully discrete setting, some implicitness or very small steps sizes are typically required for stability.

Local adaptivity and mesh refinement are certainly key to the efficient numerical solution of PDEs with heterogeneous media or complex geometry. Locally refined meshes, however, also cause a severe bottleneck for any standard explicit time integration, as the maximal time-step is dictated by maybe a few small elements in the mesh. To overcome the crippling effect of local mesh refinement, various multirate (or local time-stepping) methods [21] were proposed following the original local adaptive mesh refinement (AMR) strategy for first-order hyperbolic conservation laws by Berger and Olinger [8] — see [18] for a review. For parabolic problems, Ewing et al. [16, 17] derived and analyzed implicit finite difference schemes when local refinement is utilized in space and time. Dawson, Du and Dupont [9] combined implicit time integration in subdomains with an explicit treatment of the interfaces, which leads to a decoupled but conditionally stable system. In [40, 52], various predictor-corrector and domain decomposition methods were combined to iteratively correct the solution or its boundary values at artificial interfaces. By using static-regridding, Trompert and Verwer [55, 56, 57, 58] developed a number of multirate time-stepping strategies for local uniform grid refinement (LUGR), where a first integration is performed on a global coarse grid and the accuracy is iteratively improved locally on nested and increasingly finer subgrids.

In contrast to the above implicit, or locally implicit, multirate strategies, fully explicit RKC time integration was recently combined with the AMR approach [5, 41] to tackle diffusion dominated problems. Again, the mesh is divided into two distinct regions, the “coarse region,” which contains the larger elements and corresponds to the mildly stiff part f_S , and the “fine region,” which contains the smallest elements and thus corresponds to the severely stiff component f_F . In either subregion, the number of stages s is chosen according to the local mesh size, while “ghost cell” values at the coarse-to-fine interface are obtained by interpolating in time between stage values. For certain problems, however, time interpolation of missing stage values from the other RKC method can cause numerical instabilities [5].

To overcome the stringent stability condition due to a few severely stiff degrees of freedom, we first introduce in Section 2 a *modified equation*, where the spectral radius of its right-hand side, or *averaged force*, is bounded by that of the slower term f_S yet still remains a good approximation of (1.1). Evaluation of this averaged force requires the solution to a stiff, but cheap, auxiliary problem over short time and forms the basis of our multirate strategy. In fact, the numerical integration of the modified equation by any explicit method via such a multirate approach will be more efficient than integrating (1.1) directly with the same explicit method. In Section 3, we devise a multirate Runge–Kutta–Chebyshev (RKC) method explicit in both the fast and slow scales by utilizing two different RKC methods to integrate the modified equation and evaluate the averaged force. The resulting multirate RKC (mRKC) method assumes no scale separation, requires no interpolation between stages, and remains accurate even if the roles of f_F and f_S change in time. The fully discrete stability and accuracy analysis of the mRKC scheme is given in Section 4. Finally, in Section 5, we apply our mRKC method to a series of test problems from both stiff ordinary and partial differential equations to demonstrate its usefulness and efficiency.

2 Averaged force, modified equation and multirate algorithm

First, we introduce the *modified equation* where f in (1.1) is replaced by an *averaged force*, f_η , which depends on a free parameter $\eta \geq 0$. For $\eta = 0$ it holds $f_\eta = f$ whereas for $\eta > 0$, the spectrum of f_η is compressed and thus f_η is less stiff than f , see Figure 2. In fact for $\eta > 0$ sufficiently large, the spectral radius ρ_η of the Jacobian of f_η is bounded by the spectral radius ρ_S of the Jacobian of f_S , i.e. $\rho_\eta \leq \rho_S$; then, the stiffness of the modified equation depends solely on f_S and its integration by any explicit method is cheaper than (1.1) integrated with the same method. Since the condition $\rho_\eta \leq \rho_S$ is already satisfied for η relatively small, f_η actually remains a good approximation of f . Next, we devise a multirate strategy based on the modified equation, which is implemented in Section 3 using two separate RKC methods. Finally, we analyze the properties of f_η , derive a priori error bounds for the solution of the modified equation and perform a stability analysis.

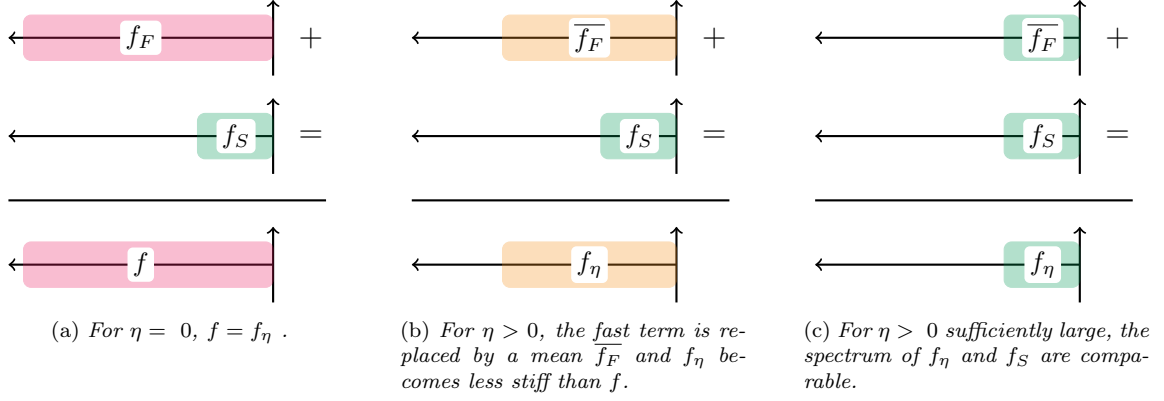


Figure 2. Spectrum of f and of the averaged force f_η for varying η .

2.1 Averaged force and modified equation

We now define an average f_η of f such that the solution y_η of the modified equation,

$$y'_\eta = f_\eta(y_\eta), \quad y_\eta(0) = y_0 \quad (2.1)$$

is a good approximation of the exact solution y of (1.1), yet the stiffness of (2.1) only depends on f_S .

Definition 2.1. For $\eta > 0$, the averaged force $f_\eta : \mathbb{R}^n \rightarrow \mathbb{R}^n$ is defined as

$$f_\eta(y) = \frac{1}{\eta} (u(\eta) - y), \quad (2.2)$$

where the auxiliary solution $u : [0, \eta] \rightarrow \mathbb{R}^n$ is defined by the auxiliary equation

$$u' = f_F(u) + f_S(y), \quad u(0) = y. \quad (2.3)$$

For $\eta = 0$, let $f_0 = f$ (note that $f_0 = \lim_{\eta \rightarrow 0^+} f_\eta$).

Therefore, whenever $f_\eta(y_\eta(t))$ is evaluated in (2.1), the auxiliary problem (2.3) must be solved over the time interval $[0, \eta]$ with initial value $u(0) = y_\eta(t)$. From (2.2) and (2.3), it follows that

$$f_\eta(y) = \frac{1}{\eta} \int_0^\eta u'(s) ds = f_S(y) + \frac{1}{\eta} \int_0^\eta f_F(u(s)) ds.$$

Hence, f_η is an average of f over the time interval $[0, \eta]$ along the auxiliary solution u . For η sufficiently large, we show in Section 2.3 that $\rho_\eta \leq \rho_S$.

Multirate strategy. Starting from the modified equation (2.1), we propose the following explicit multirate strategy for the numerical approximation of (1.1): Solve (2.1) with an explicit numerical method, where stability conditions depend on f_S only. Whenever an evaluation of f_η is needed, (2.3) is solved with a (possibly different) explicit method, with stability conditions depending on f_F . Since f_F is cheap, evaluating f_η in (2.1) by solving (2.3) carries about the same computational cost as evaluating f in (1.1). On the other hand, since the stiffness, and hence the step size, needed for (2.1) no longer depends on the fastest scales in the problem, the number of expensive f_S evaluations will be greatly reduced.

Although the above multirate strategy might at first resemble recently introduced multiscale methods, such as HMM for dissipative ODEs, it is fundamentally different because the averaged equation (2.1) requires no scale separation: both f_S and f_F may contain slow scales, in contrast to the effective equations derived in [12], for instance. The above multirate strategy might also resemble

multirate infinitesimal step (MIS) methods [34, 65]. MIS methods, however, only discretize the slow variables while assuming the fast dynamics to be integrated exactly; hence, the fast variables do not produce any instability. In contrast, the multirate methods introduced here discretize the modified equation (2.1), where the spectrum of the fast dynamics has been compressed. Moreover, we provide a fully discrete stability and accuracy analysis below. Finally, an auxiliary problem similar to (2.3) also appears in the context of second-order ODEs [30] (see also [27, VIII.4.2]). In [30], however, the auxiliary problem is integrated over the entire interval $[-\tau, \tau]$ using smaller step sizes τ/N , while y_{n+1}, y'_{n+1} are defined through finite difference approximations of u . In contrast, here we solve (2.3) over the small time interval $[0, \eta]$ with $\eta \ll \tau$, while u is used to compute f_η , which in turn defines the equation for y_η .

2.2 A priori error analysis for the solution of the modified equation

Here we analyze the effect of the parameter η on f_η and show that f_η satisfies a one-sided Lipschitz condition, which is fundamental for proving convergence and contractivity for general nonlinear problems [29, IV.12]. Then, we derive bounds on the error introduced by solving (2.1) instead of (1.1), which are independent of the problem's stiffness.

Let $\langle \cdot, \cdot \rangle$ and $\|\cdot\|$ denote the standard Euclidean scalar product and norm in \mathbb{R}^n , respectively. To begin, we prove that f_F has a smoothing effect on f_η , if it satisfies a one-sided Lipschitz condition.

Lemma 2.2. *Let $\mu_F \in \mathbb{R}$ and f_F satisfy*

$$\langle f_F(z) - f_F(y), z - y \rangle \leq \mu_F \|z - y\|^2 \quad \forall z, y \in \mathbb{R}^n. \quad (2.4)$$

Then

$$\|f_\eta(y)\| \leq \varphi(\eta\mu_F) \|f(y)\|, \quad \text{where} \quad \varphi(z) = \frac{e^z - 1}{z} \quad \text{for } z \neq 0 \quad (2.5)$$

and $\varphi(0) = 1$ is defined by continuous extension. Moreover, if $f_F(y) = A_F y$ with $A_F \in \mathbb{R}^{n \times n}$, then

$$f_\eta(y) = \varphi(\eta A_F) f(y). \quad (2.6)$$

Proof. Let $v : [0, \eta] \rightarrow \mathbb{R}^n$ be defined by $v(s) = y$ for all s . We set

$$\delta := \|v'(s) - f_F(v(s)) - f_S(y)\| = \|f(y)\|.$$

Since the logarithmic norm of the Jacobian of f_F is bounded by μ_F , we obtain from a classical result on differential inequalities (see [28, Chapter I.10, Theorem 10.6])

$$\|u(\eta) - y\| = \|u(\eta) - v(\eta)\| \leq e^{\eta\mu_F} \int_0^\eta e^{-s\mu_F} \delta \, ds = \eta \varphi(\eta\mu_F) \|f(y)\|,$$

which yields (2.5) by (2.2). Now, let $f_F(u) = A_F u$ with $A_F \in \mathbb{R}^{n \times n}$ nonsingular. Then, the variation-of-constants formula with $f_F(u) = A_F u$ in (2.3) yields

$$u(\eta) = e^{A_F \eta} \left(y + \int_0^\eta e^{-A_F s} f_S(y) \, ds \right) = e^{A_F \eta} y + A_F^{-1} (e^{A_F \eta} - I) f_S(y),$$

with I the identity matrix. Hence,

$$u(\eta) = e^{A_F \eta} y + \eta \varphi(\eta A_F) f_S(y). \quad (2.7)$$

Since φ has no poles, $u(\eta)$ as in (2.7) is well-defined and satisfies (2.3) for all matrices A_F . By using (2.2), we thus obtain

$$f_\eta(y) = \frac{1}{\eta} (e^{A_F \eta} - I) y + \varphi(\eta A_F) f_S(y) = \varphi(\eta A_F) (A_F y + f_S(y)) = \varphi(\eta A_F) f(y). \quad \square$$

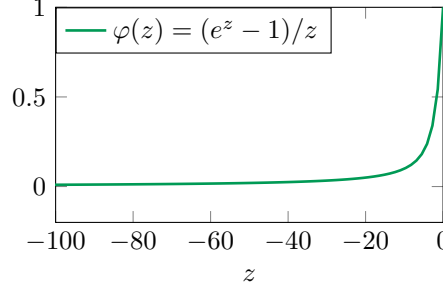


Figure 3. The entire function $\varphi(z)$.

Remark 2.3. The entire function $\varphi(z)$ is quite common in the theory of exponential integrators [31]. Indeed, when $f_F(y) = A_F y$, the solution (2.7) to the auxiliary problem (2.3) corresponds to a single step of the exponential Euler method applied to (1.1). Our multirate approach, however, differs from exponential integrators: First, $u(\eta)$ is just an auxiliary solution used to compute f_η , which is distinct from the solution y_η of the modified equation (2.1). Second, we do not use an exponential integrator but an RKC method to obtain $u(\eta)$; thus, $\varphi(\eta A_F)$ is never computed explicitly. Third, η is not the step size here but a free parameter indicating the length of the integration interval in (2.3).

The function $\varphi(z)$, shown in Figure 3, satisfies

$$\varphi(0) = 1, \quad \varphi'(0) = \frac{1}{2}, \quad \lim_{z \rightarrow -\infty} \varphi(z) = 0, \quad 0 < \varphi(z) < 1, \quad \forall z < 0.$$

Hence, if A_F is negative definite, multiplication of f by $\varphi(\eta A_F)$ in (2.6) has a smoothing effect, which can be tuned by varying $\eta \geq 0$ — see Theorem 2.7 below. A similar property holds for any nonlinear f_F that is contractive, i.e. with $\mu_F \leq 0$ in (2.4), because of (2.5).

Next, we prove under the assumption that the Jacobians of f_F and f_S commute that the averaged force f_η satisfies a one-sided Lipschitz condition. Clearly, commutativity of the Jacobians is a rather strong assumption, rarely satisfied in practice. It is merely used here to provide insight into the behavior of f_η and in fact not needed when subsequently applying the multirate method.

Theorem 2.4. Let $A_F \in \mathbb{R}^{n \times n}$ be symmetric and $f_F(y) = A_F y$. Suppose

$$\left\langle \frac{\partial f}{\partial y}(w)(z - y), z - y \right\rangle \leq \mu \|z - y\|^2 \quad \forall w, y, z \in \mathbb{R}^n \quad (2.8)$$

with $\mu \leq 0$ and that $A_F \frac{\partial f_S}{\partial y}(w) = \frac{\partial f_S}{\partial y}(w) A_F$ for all $w \in \mathbb{R}^n$. Then,

$$\langle f_\eta(z) - f_\eta(y), z - y \rangle \leq \mu_\eta \|z - y\|^2,$$

where $\mu_\eta = \mu \min_{\lambda \in \lambda(A_F)} \{\varphi(\eta \lambda)\} \leq 0$ and $\lambda(A_F)$ is the spectrum of A_F .

Proof. Let $y, z \in \mathbb{R}^n$ and $w(r) = rz + (1 - r)y$ for $r \in [0, 1]$. We have

$$\begin{aligned} \langle f_\eta(z) - f_\eta(y), z - y \rangle &= \langle \varphi(\eta A_F)(f(z) - f(y)), z - y \rangle \\ &= \langle \varphi(\eta A_F)^{1/2} \int_0^1 \frac{\partial f}{\partial y}(w(r))(z - y) dr, \varphi(\eta A_F)^{1/2}(z - y) \rangle. \end{aligned}$$

Since $\varphi(z) > 0$ for all z , $\varphi(\eta A_F)$ is symmetric positive definite and $\varphi(\eta A_F)^{1/2}$ exists. By hypothesis, $\varphi(\eta A_F)^{1/2}$ and $\frac{\partial f}{\partial y}(w(r))$ commute. Therefore

$$\begin{aligned} \langle f_\eta(z) - f_\eta(y), z - y \rangle &= \int_0^1 \left\langle \frac{\partial f}{\partial y}(w(r)) \varphi(\eta A_F)^{1/2}(z - y), \varphi(\eta A_F)^{1/2}(z - y) \right\rangle dr \\ &\leq \mu \|\varphi(\eta A_F)^{1/2}(z - y)\|^2 \leq \mu \min_{\lambda \in \lambda(A)} \{\varphi(\eta \lambda)\} \|z - y\|^2. \quad \square \end{aligned}$$

Theorem 2.4 shows that f_η indeed satisfies a one-sided Lipschitz condition, if the Jacobians of f_F , f_S commute and (2.8) holds, which is slightly stronger than requiring that f satisfies a one-sided Lipschitz condition. Indeed, f is one-sided Lipschitz if, and only if, (2.8) holds for all z, y and $w \in [z, y]$, see [28, I.10]. Next, we bound the error between the solutions of (1.1) and (2.1).

Theorem 2.5. *Under the assumptions of Theorem 2.4, it holds*

$$\|y(t) - y_\eta(t)\| \leq \max_{\lambda \in \lambda(A_F)} |1 - \varphi(\eta\lambda)| \int_0^t e^{\mu_\eta(t-s)} \|f(y(s))\| ds, \quad (2.9)$$

with $\mu_\eta = \mu \min_{\lambda \in \lambda(A_F)} \{\varphi(\eta\lambda)\} \leq 0$.

Proof. Let $y(t)$ be the solution to (1.1). From Lemma 2.2, we have

$$\begin{aligned} \|y'(t) - f_\eta(y(t))\| &= \|f(y(t)) - f_\eta(y(t))\| = \|(I - \varphi(\eta A_F))f(y(t))\| \\ &\leq \max_{\lambda \in \lambda(A_F)} |1 - \varphi(\eta\lambda)| \|f(y(t))\| =: \delta(t). \end{aligned}$$

Since the logarithmic norm of the Jacobian of f_η is bounded by $\mu_\eta = \mu \min_{\lambda \in \lambda(A_F)} \{\varphi(\eta\lambda)\}$, as implied by Theorem 2.4, the estimate (2.9) follows from classical results on differential inequalities (see [28, Chapter I.10, Theorem 10.6]). \square

Note that the error bound (2.9) is independent of the stiffness present in f_F and that $\|y(t) - y_\eta(t)\| \leq C\eta$ as $\eta \rightarrow 0$ because $\varphi(\eta\lambda) = 1 + \mathcal{O}(\eta)$.

2.3 Stability analysis of the modified equation

We now study the stiffness of the modified equation (2.1) given by the spectral radius ρ_η of the Jacobian of f_η . In particular, we determine necessary conditions for $\rho_\eta \leq \rho_S$, with ρ_S the spectral radius of the Jacobian of f_S , and hence that the stiffness of the modified equation only depends on the slow components. As in Theorem 2.4, we assume that the Jacobians of f_F and f_S commute. In Section 4, we shall analyze the stability of our multirate method, first under the same commutativity assumption but then also for a 2×2 problem where the Jacobians do not commute. For more general problems, stability is verified numerically in Section 5.

Let the Jacobians of f_F and f_S commute. Then, they are simultaneously triangularizable and the stability analysis of (1.1) and (2.1) reduces to the scalar *multirate test equation*

$$y' = \lambda y + \zeta y, \quad y(0) = y_0, \quad (2.10)$$

with $\lambda, \zeta \leq 0$ and $y_0 \in \mathbb{R}$, which corresponds to setting $f_F(y) = \lambda y$ and $f_S(y) = \zeta y$; thus, $\rho_F = |\lambda|$ and $\rho_S = |\zeta|$. Since we do not assume any scale separation, λ can take any nonpositive value.

Since (2.10) satisfies the hypotheses of Lemma 2.2 with $\mu_F = A_F = \lambda$, we have

$$u(\eta) = (e^{\eta\lambda} + \varphi(\eta\lambda)\eta\zeta)y, \quad (2.11)$$

$$f_\eta(y) = \varphi(\eta\lambda)(\lambda + \zeta)y \quad (2.12)$$

and (2.1) reduces to

$$y'_\eta = \varphi(\eta\lambda)(\lambda + \zeta)y_\eta, \quad y_\eta(0) = y_0. \quad (2.13)$$

Next, we determine conditions on η, λ and ζ which guarantee that

$$|\varphi(\eta\lambda)(\lambda + \zeta)| \leq |\zeta|,$$

and hence that the stiffness of (2.13) exclusively depends on $\rho_S = |\zeta|$. The following technical lemma is used to prove Theorem 2.7 below.

Lemma 2.6. *Let $w \leq 0$ and $\varphi(z)$ be given by (2.5). Then, $\varphi(z)(z + w) \in [w, 0]$ for all $z \leq 0$ if, and only if, $\varphi'(0)|w| \geq 1$, i.e. $|w| \geq 2$ since $\varphi'(0) = 1/2$.*

Proof. For $z, w \leq 0$, the upper bound $\varphi(z)(z+w) \leq 0$ always holds. Hence, we only need to consider the lower bound,

$$\varphi(z)(z+w) \geq w. \quad (2.14)$$

Suppose that (2.14) holds for all $z \leq 0$. In a neighborhood of $z = 0$, this yields

$$\begin{aligned} 0 &\leq \varphi(z)(z+w) - w = (\varphi(0) + \varphi'(0)z + \mathcal{O}(z^2))(z+w) - w \\ &= z(1 + \varphi'(0)(z+w)) + \mathcal{O}(z^2(z+w)), \end{aligned} \quad (2.15)$$

where we have used that $\varphi(0) = 1$. Dividing (2.15) by $z < 0$ and letting $z \rightarrow 0$ yields $\varphi'(0)w \leq -1$, and thus $\varphi'(0)|w| \geq 1$.

Now, let $\varphi'(0)|w| \geq 1$ and hence $w \leq -1/\varphi'(0) = -2$. For $z = 0$, (2.14) trivially holds. For $z < 0$, we multiply (2.14) by z and prove the resulting equivalent condition:

$$\alpha(z) = zw + (1 - e^z)(z+w) \geq 0 \quad \forall z < 0.$$

Since

$$\alpha'(z) = 1 + w - (1 + w + z)e^z, \quad \alpha''(z) = -(2 + w + z)e^z,$$

we have $\alpha(0) = \alpha'(0) = 0$. Since $w \leq -2$, we have

$$\alpha(z) = \int_0^z \int_0^s \alpha''(r) dr ds = - \int_z^0 \int_s^0 (2 + w + r)e^r dr ds \geq 0,$$

which concludes the proof. \square

Theorem 2.7. *Let $\zeta < 0$. Then, $\varphi(\eta\lambda)(\lambda + \zeta) \in [\zeta, 0]$ for all $\lambda \leq 0$ if, and only if, $\eta \geq 2/|\zeta|$.*

Proof. Setting $z = \eta\lambda$ and $w = \eta\zeta$, we have that

$$\varphi(\eta\lambda)(\lambda + \zeta) \in [\zeta, 0] \quad \text{is equivalent to} \quad \varphi(z)(z+w) \in [w, 0].$$

In view of Lemma 2.6, this holds for all $\lambda \leq 0$, if and only if $\eta|\zeta| = |w| \geq 2$. \square

Theorem 2.7 implies that for $\eta \geq 2/\rho_S$ the stiffness of (2.13) depends only on the slow term f_S . Since η does not depend on λ and the result holds for all $\lambda \leq 0$, there is no need for any assumption on scale separation.

3 A stabilized method based on the modified equation: the multirate Runge–Kutta–Chebyshev method

Although the modified equation (2.1) has reduced stiffness, implementing a multirate strategy based on (2.1) and (2.3) with classical explicit methods remains inefficient, as it will lead to step size restrictions due to their inherent stiffness. Instead, we introduce here the mRKC method, which is based on two RKC methods and thus has no step size restrictions. Moreover, thanks to the multirate strategy, the number of f_S (expensive) evaluations is independent of the stiffness of f_F and thus no longer suffers from the efficiency loss of any classical stabilized scheme. In Section 3.1 we briefly recall some basic definitions and properties of the RKC scheme before introducing the mRKC method in Section 3.2

3.1 Stabilized Runge–Kutta methods

Stabilized Runge–Kutta methods [1, 2, 36, 37, 39, 54, 59, 64] are explicit one-step Runge–Kutta (RK) methods with an extended stability domain along the negative real axis. By increasing the number of stages, with respect to classical RK methods, they relax the stringent constraint of standard explicit RK methods on the step size. Their construction relies on Chebyshev polynomials of the first kind,

$T_s(x)$, and the classical first-order family of methods, the Runge–Kutta–Chebyshev (RKC) methods [59, 64], is given by the s -stage RK method

$$\begin{aligned} k_0 &= y_n, \\ k_1 &= k_0 + \mu_1 \tau f(k_0), \\ k_j &= \nu_j k_{j-1} + \kappa_j k_{j-2} + \mu_j \tau f(k_{j-1}) \quad j = 2, \dots, s, \\ y_{n+1} &= k_s, \end{aligned} \tag{3.1}$$

where τ is the step size, $\mu_1 = \omega_1/\omega_0$ and

$$\mu_j = 2\omega_1 b_j / b_{j-1}, \quad \nu_j = 2\omega_0 b_j / b_{j-1}, \quad \kappa_j = -b_j / b_{j-2} \quad \text{for } j = 2, \dots, s, \tag{3.2}$$

with $\varepsilon \geq 0$, $\omega_0 = 1 + \varepsilon/s^2$, $\omega_1 = T_s(\omega_0)/T'_s(\omega_0)$ and $b_j = 1/T_j(\omega_0)$ for $j = 0, \dots, s$. We note that the explicit Euler method is recovered for $s = 1$.

When applied to the test equation $y' = \lambda y$ and using

$$T_0(x) = 1, \quad T_1(x) = x, \quad T_j(x) = 2xT_{j-1}(x) - T_{j-2}(x),$$

(3.1) yields $y_{n+1} = R_s(z)y_n$, where $z = \tau\lambda$ and

$$R_s(z) = b_s T_s(\omega_0 + \omega_1 z) \tag{3.3}$$

is the stability polynomial of the method. As $T_s(x) \geq 1$ for $x \geq 1$ and $|T_s(x)| \leq 1$ for $x \in [-1, 1]$ then $|R_s(z)| \leq 1$ for $z \in [-\ell_s^\varepsilon, 0]$ and $\ell_s^\varepsilon = 2\omega_0/\omega_1$. As $\beta s^2 \leq \ell_s^\varepsilon$, for $\beta = 2 - 4\varepsilon/3$, then $|z| \leq \beta s^2$ is a sufficient condition for stability [63] and the stability domain

$$\mathcal{S} = \{z \in \mathbb{C} : |R_s(z)| \leq 1\}$$

increases quadratically, with respect to the stage number s , along the negative real axis (see Figure 4(b)). The parameter $\varepsilon \geq 0$ is a damping parameter introduced to increase stability in the imaginary direction [23] (compare Figures 4(a) and 4(b) for $s = 10$). In Figure 4(c) we also plot the stability polynomial of the RKC scheme for different values of s and ε , observe as the stability domain increases quadratically with s and as the polynomials satisfy $|R_s(z)| < 1$ for $\varepsilon > 0$.

For a general right-hand side $f : \mathbb{R}^n \rightarrow \mathbb{R}^n$ the number of stages s in (3.1) is typically chosen such that $\tau\rho \leq \beta s^2$, where ρ is the spectral radius of the Jacobian of f . In (3.1) and below, we consider autonomous problems for convenience only and refer to [64] for the RKC method in nonautonomous form. The three term recurrence relation allow for low memory requirements even for very large s and good internal stability properties [59].

3.2 The multirate RKC method

The multirate RKC scheme is obtained by discretizing (2.1) with an s -stage RKC method, where f_η , given by Definition 2.1, is approximated by solving problem (2.3) with one step of an m -stage RKC method. In this section, we first define the mRKC algorithm and then compare its efficiency to that of the standard RKC method (3.1).

The mRKC Algorithm

Let $\tau > 0$ be the step size and ρ_F, ρ_S the spectral radii of the Jacobians of f_F, f_S , respectively (they can be cheaply estimated employing nonlinear power methods [38, 62]). Now, let the number of stages s, m be the smallest integers satisfying

$$\tau\rho_S \leq \beta s^2, \quad \eta\rho_F \leq \beta m^2, \quad \text{with} \quad \eta = \frac{6\tau}{\beta s^2} \frac{m^2}{m^2 - 1}, \tag{3.4}$$

for the standard RKC parameter settings $\beta = 2 - 4\varepsilon/3$ and $\varepsilon = 0.05$ – see Section 3.1. The value for η will be clear from the stability analysis in Section 4.1.

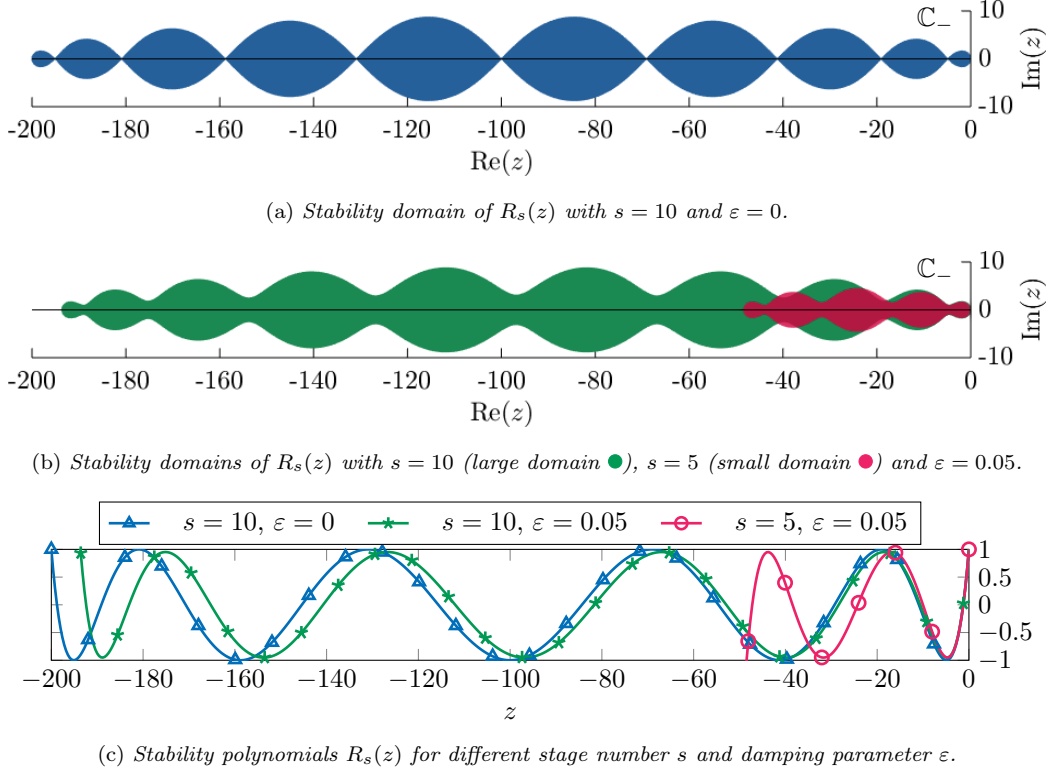


Figure 4. Stability domains and polynomials of the RKC method, for different stage number s and damping ε .

One step of the mRKC scheme is then given by

$$\begin{aligned}
 k_0 &= y_n, \\
 k_1 &= k_0 + \mu_1 \tau \bar{f}_\eta(k_0), \\
 k_j &= \nu_j k_{j-1} + \kappa_j k_{j-2} + \mu_j \tau \bar{f}_\eta(k_{j-1}) \quad j = 2, \dots, s, \\
 y_{n+1} &= k_s,
 \end{aligned} \tag{3.5}$$

where the parameters μ_j, ν_j, κ_j are defined in (3.2) and

$$\bar{f}_\eta(y) = \frac{1}{\eta} (u_\eta - y) \tag{3.6}$$

corresponds to the numerical counterpart of $f_\eta(y)$ in (2.2). The approximation u_η of $u(\eta)$ is computed at each evaluation of \bar{f}_η by applying one step, of size η , of the m -stage RKC scheme to (2.3). Hence, u_η is given by

$$\begin{aligned}
 u_0 &= y, \\
 u_1 &= u_0 + \alpha_1 \eta (f_F(u_0) + f_S(y)), \\
 u_j &= \beta_j u_{j-1} + \gamma_j u_{j-2} + \alpha_j \eta (f_F(u_{j-1}) + f_S(y)) \quad j = 2, \dots, m, \\
 u_\eta &= u_m.
 \end{aligned} \tag{3.7}$$

Here, the parameters $\alpha_j, \beta_j, \gamma_j$ of the m -stage RKC scheme (3.7) are given by

$$v_0 = 1 + \varepsilon/m^2, \quad v_1 = T_m(v_0)/T'_m(v_0), \quad a_j = 1/T_j(v_0) \quad \text{for } j = 0, \dots, m \tag{3.8}$$

and $\alpha_1 = v_1/v_0$,

$$\alpha_j = 2v_1 a_j / a_{j-1}, \quad \beta_j = 2v_0 a_j / a_{j-1}, \quad \gamma_j = -a_j / a_{j-2} \quad \text{for } j = 2, \dots, m.$$

To compute m, η in (3.4), we let $\eta = 6\tau m^2/(\beta s^2(m^2 - 1))$ in $\eta\rho_F \leq \beta m^2$, which implies

$$6\tau\rho_F \leq \beta^2 s^2(m^2 - 1). \quad (3.9)$$

Thus, we use (3.9) to compute m and then (3.4) to determine η .

The mRKC method is given by (3.4)–(3.7). Its stability and first-order accuracy are proved in Theorems 4.5 and 4.6 in Section 4 below.

Efficiency of the multirate RKC method

Given the spectral radii ρ_F and ρ_S of the Jacobians of f_F and f_S , respectively, we now evaluate the theoretical speed-up in using the mRKC method (3.4) to (3.7) over the standard RKC method (3.1). In doing so, we set $\varepsilon = 0$ and let s, m vary in \mathbb{R} . Now, we let c_F and c_S denote the cost of evaluating f_F and f_S , relatively to the cost of evaluating f itself, with $c_F, c_S \in [0, 1]$ and $c_F + c_S = 1$. Here, we suppose that the spectral radius ρ of the Jacobian of f is $\rho = \rho_F + \rho_S$, instead of setting $\rho = \rho_F$, to allow for a wide range of possible values for ρ_F even down to zero.

Since the RKC scheme requires $s = \sqrt{\tau\rho/2}$ evaluations of f per time step, its cost per time step is

$$C_{\text{RKC}} = s(c_F + c_S) = \sqrt{\frac{\tau(\rho_F + \rho_S)}{2}}. \quad (3.10)$$

For the mRKC method, on the other hand, we infer from (3.4) with $\beta = 2$ that it needs $s = \sqrt{\tau\rho_S/2}$ external stages and from (3.9) that it needs $m = \sqrt{3\rho_F/\rho_S + 1}$ internal stages. Since mRKC needs s evaluations of f_S and sm evaluations of f_F , its cost per time step is

$$C_{\text{mRKC}} = s c_S + s m c_F = (1 - c_F) \sqrt{\frac{\tau\rho_S}{2}} + c_F \sqrt{\frac{3\tau\rho_F}{2} + \frac{\tau\rho_S}{2}}. \quad (3.11)$$

The ratio between (3.10) and (3.11) yields the *relative speed-up*

$$S = \frac{C_{\text{RKC}}}{C_{\text{mRKC}}} = \frac{\sqrt{\rho_F + \rho_S}}{(1 - c_F)\sqrt{\rho_S} + c_F\sqrt{\rho_S + 3\rho_F}} = \frac{\sqrt{1 + r_\rho}}{1 + c_F(\sqrt{1 + 3r_\rho} - 1)}, \quad (3.12)$$

with *stiffness ratio* $r_\rho = \rho_F/\rho_S \in [0, \infty)$.

In Figure 5(a), we show the speed-up S as a function of c_F for different values of $r_\rho = \rho_F/\rho_S$. For c_F sufficiently small, we observe that the mRKC scheme is always faster than RKC ($S > 1$). When $c_F \approx 1$, however, the mRKC scheme is slightly slower than RKC ($S < 1$), though this case is somewhat irrelevant since by assumption f_F is cheap to evaluate. Nevertheless, we solve the inequality $S > 1$, with S as in (3.12), for varying c_F to determine the maximal value of c_F that still leads to a reduced cost in using mRKC. We find that the speed-up $S > 1$ if, and only if,

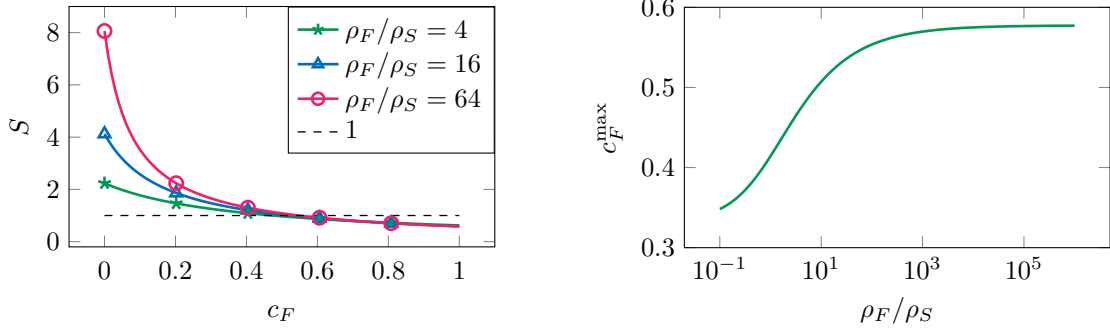
$$c_F < c_F^{\max} = \frac{\sqrt{1 + r_\rho} - 1}{\sqrt{1 + 3r_\rho} - 1}.$$

In Figure 5(b), we monitor c_F^{\max} as a function of the stiffness ratio r_ρ . For small $r_\rho = \rho_F/\rho_S$, we observe that the evaluation of f_F must be quite cheap. As ρ_F/ρ_S increases, however, the mRKC method is faster than RKC, even if f_F is relatively expensive to evaluate ($c_F^{\max} > 0.5$ for $\rho_F/\rho_S > 8$).

Relaxed stability conditions

The stability conditions (3.4) are necessary when solving a general problem (1.1) without any scale separation. However, in case of scale separation ($\lambda \ll \zeta$), conditions (3.4) can in fact be replaced by

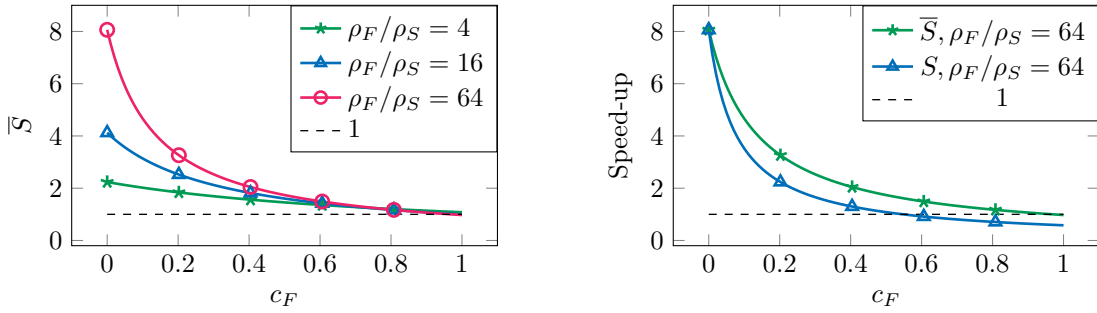
$$\tau\rho_S \leq \beta s^2, \quad \eta\rho_F \leq \bar{\beta}m^2 \quad \text{with} \quad \eta = \frac{2\tau}{\beta s^2}, \quad (3.13)$$



(a) Theoretical speed-up S of the mRKC method over the standard RKC scheme, with respect to c_F and ρ_F/ρ_S .

(b) Maximal c_F which still yields speed-up $S > 1$, w.r.t. ρ_F/ρ_S .

Figure 5. The relative speed-up S of the mRKC method over the RKC scheme with respect to c_F and the maximal value for c_F which still leads to an efficiency gain.



(a) Theoretical speed-up \bar{S} of the mRKC method over the standard RKC scheme, with respect to c_F and ρ_F/ρ_S .

(b) Comparison of \bar{S} and S .

Figure 6. The relative speed-up \bar{S} obtained using (3.13) compared to S , obtained with (3.4).

$\bar{\beta} = 2 - 4\bar{\varepsilon}/3 \approx 1.86$ and $\bar{\varepsilon} = 0.1$ – see Remark 4.4 for further insight on the derivation of (3.13). Since the value for η in (3.13) is smaller than that in (3.4), m can also be smaller which results in fewer evaluations of f_F in (3.7) and improved efficiency. Let \bar{S} be the relative speed-up in using (3.13) instead of (3.4). In Figure 6(a), we plot \bar{S} as a function of c_F for different values of ρ_F/ρ_S , as in Figure 5(a) for S . We observe that $\bar{S} > 1$ for all $c_F \in [0, 1 - \epsilon]$, for $\epsilon > 0$ very small. In Figure 6(b), we compare S and \bar{S} and observe that $\bar{S} > S$ for all values of c_F .

Even when the underlying problem is not scale separable, conditions (3.13) may in fact be sufficient to guarantee the stability of the mRKC scheme. For instance, if (1.1) stems from the spatial discretization of a parabolic problem on a locally refined mesh, where f_S and f_F correspond to the discrete Laplacians in the coarse and locally refined region, and the problem thus is not scale separable, (3.13) nonetheless suffices to guarantee stability — see Section 5.5.

4 Stability and convergence analysis

In this section, we perform a stability and convergence analysis of the multirate RKC method introduced in Section 3. We will show stability of the scheme on the multirate test equation (2.10) and on a 2×2 model problem. Then we prove its first-order accuracy.

4.1 Stability analysis

First, we prove that the mRKC method is stable when it is applied to the multirate test equation (2.10), which is sufficient when the Jacobians of f_F and f_S are simultaneously triangularizable.

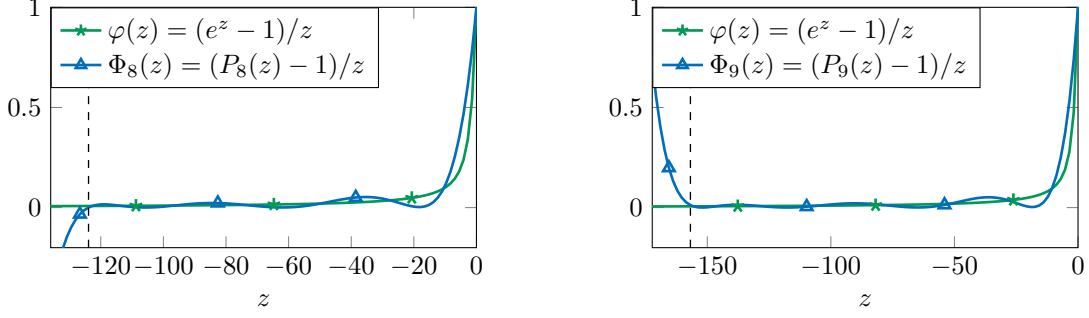


Figure 7. Illustration of $\varphi(z)$ and $\Phi_m(z)$ for $m = 8$ (left) and $m = 9$ (right). The dashed line indicates the end of the stability domain.

Then, we also show stability for a 2×2 model problem where the Jacobians of f_F and f_S are not simultaneously triangularizable, and hence the stability analysis cannot be reduced to (2.10).

Stability analysis for the multirate test equation

Since (2.3) is approximated numerically, the stability analysis performed in Section 2.3 is no longer valid; indeed, $\varphi(z)$ is now replaced by a numerical approximation with different stability properties. Hence, we now compute a closed expression for u_η given y , as in (2.11) for $u(\eta)$. We denote by

$$P_m(z) = a_m T_m(v_0 + v_1 z) \quad (4.1)$$

the stability polynomial of the m -stage RKC scheme, with a_m, v_0, v_1 from (3.8). The next lemma computes the solution u_η of (3.7) in the case of the multirate test equation (2.10).

Lemma 4.1. *Let $\lambda, \zeta \leq 0$, $f_S(y) = \zeta y$, $f_F(y) = \lambda y$, $\eta > 0$, $m \in \mathbb{N}$ and $y \in \mathbb{R}$. Then, the solution u_η of (3.7), is given by*

$$u_\eta = (P_m(\eta\lambda) + \Phi_m(\eta\lambda)\eta\zeta)y, \quad (4.2)$$

where $P_m(z)$ is given in (4.1),

$$\Phi_m(z) = \frac{P_m(z) - 1}{z} \quad \text{for } z \neq 0 \quad (4.3)$$

and $\Phi_m(0) = 1$ is defined by continuous extension.

Proof. A generalization of [29, Proposition 3.1] to the equation $u' = \lambda u + \zeta y$ (instead of $u' = \lambda u$) yields

$$u_\eta = P_m(z)y + \eta b^\top (I - zA)^{-1} \mathbf{1} \zeta y,$$

where $z = \eta\lambda$, $I \in \mathbb{R}^{m \times m}$ is the identity matrix, A, b are the coefficients of the Butcher tableau of the m -stage RKC scheme and $\mathbf{1} \in \mathbb{R}^m$ is a vector of ones. Since $P_m(z) = 1 + zb^\top (I - zA)^{-1} \mathbf{1}$ [29, Proposition 3.1] the result follows. \square

Note the similarity between (2.11) and (4.2), with $e^z, \varphi(z)$ replaced by $P_m(z), \Phi_m(z)$, respectively. In Figure 7, we also observe that $\Phi_m(z)$ and $\varphi(z)$ share similar stability properties. Indeed, $\Phi_m(z)$ is the numerical counterpart of $\varphi(z)$, yet with the exponential replaced by the stability polynomial – compare (2.5) and (4.3).

We can now compute the stability polynomial of the mRKC scheme. From (3.6), (4.2) and (4.3), we get

$$\bar{f}_\eta(y) = \frac{1}{\eta} (P_m(\eta\lambda) + \Phi_m(\eta\lambda)\eta\zeta - 1)y = \Phi_m(\eta\lambda)(\lambda + \zeta)y, \quad (4.4)$$

which is the numerical counterpart of f_η in (2.12). Now, we insert (4.4) into (3.5), which leads to

$$y_{n+1} = R_s(\tau \Phi_m(\eta\lambda)(\lambda + \zeta))y_n,$$

with $R_s(z)$ the stability polynomial of the s -stage RKC scheme defined in Section 3.1, and hence motivates the following definition.

Definition 4.2. Let $s, m \in \mathbb{N}$, $\tau > 0$ be a step size, $\eta > 0$ and $\lambda, \zeta \leq 0$. The stability polynomial of the (s, m) -stage mRKC scheme (3.5)–(3.7) is defined as

$$R_{s,m}(\lambda, \zeta, \tau, \eta) = R_s(\tau \Phi_m(\eta\lambda)(\lambda + \zeta)),$$

with $R_s(z)$ as in (3.3) and $\Phi_m(z)$ as in (4.3).

The following lemma is the discrete version of Lemma 2.6 and is needed to prove stability of the mRKC scheme in Theorem 4.5 below. Its proof is purely technical and postponed to Appendix A.

Lemma 4.3. Let $m \in \mathbb{N}$ and $w \leq 0$. There exists $\bar{\varepsilon}_m > 0$ such that for $\varepsilon \leq \bar{\varepsilon}_m$, $\Phi_m(z)(z+w) \in [w, 0]$ for all $z \in [-\ell_m^\varepsilon, 0]$ if, and only if, $\Phi'_m(0)|w| \geq 1$, i.e. $|w| \geq 2/P''_m(0)$ since $\Phi'_m(0) = P''_m(0)/2$.

For $\varepsilon = 0$, it holds $2/P''_m(0) = 6m^2/(m^2 - 1) > 6$. In the continuous setting, the condition on w in Lemma 2.6 was $|w| \geq 2$. For the discrete mRKC scheme, however, $|w| > 6$ is necessary because of the milder slope of $\Phi_m(z)$ at the origin, see Figure 7.

Remark 4.4. In the case of scale separation, z is bounded away from the origin and the value of $\Phi_m(z)$ thus considerably smaller than 1, see Figure 7. Hence, the condition $\Phi_m(z)(z+w) \in [w, 0]$ is already satisfied for $|w| \geq 2$ and a slightly larger damping $\bar{\varepsilon} = 0.1$, so that the larger value $|w| \geq 2/P''_m(0) \approx 6$, required by Lemma 4.3, is no longer necessary. By allowing $|w| \geq 2$ instead of $|w| \geq 2/P''_m(0)$ in Theorem 4.5 below, we find that the weaker stability conditions (3.13) already guarantee stability in the case of scale separation – see [45, Section 3.4.5] for further details.

Theorem 4.5. Let $\bar{\varepsilon}_m$ be as in Lemma 4.3 and, for $\varepsilon \geq 0$, let $\varepsilon_m = \min\{\varepsilon, \bar{\varepsilon}_m\}$. Let $\lambda \leq 0$ and $\zeta < 0$. Then, for all $\tau > 0, s, m$ and η such that

$$\tau|\zeta| \leq \ell_s^\varepsilon, \quad \eta|\lambda| \leq \ell_m^{\varepsilon_m} \quad \text{with} \quad \eta \geq \frac{6\tau}{\ell_s^\varepsilon} \frac{m^2}{m^2 - 1}, \quad (4.5)$$

$|R_{s,m}(\lambda, \zeta, \tau, \eta)| \leq 1$, i.e. the mRKC scheme is stable.

Proof. If $\tau \Phi_m(\eta\lambda)(\lambda + \zeta) \in [-\ell_s^\varepsilon, 0]$ then $|R_{s,m}(\lambda, \zeta, \tau, \eta)| = |R_s(\tau \Phi_m(\eta\lambda)(\lambda + \zeta))| \leq 1$. Hence, it is sufficient to prove the equivalent condition:

$$\Phi_m(\eta\lambda)(\eta\lambda + \eta\zeta) \in [w(\eta), 0], \quad \text{with} \quad w(\eta) = -\frac{\eta}{\tau} \ell_s^\varepsilon.$$

Since $\eta\lambda \in [-\ell_m^{\varepsilon_m}, 0]$, it holds $|P_m(\eta\lambda)| \leq 1$ and from (4.3) we thus deduce that $\Phi_m(\eta\lambda) \geq 0$. Furthermore, (4.5) yields $\eta\zeta \geq w(\eta)$ which implies

$$0 \geq \Phi_m(\eta\lambda)(\eta\lambda + \eta\zeta) \geq \Phi_m(z(\eta))(z(\eta) + w(\eta)),$$

with $z(\eta) = \eta\lambda$. Hence, it is sufficient to show that $\Phi_m(z(\eta))(z(\eta) + w(\eta)) \in [w(\eta), 0]$ for all $z(\eta) \in [-\ell_m^{\varepsilon_m}, 0]$. From Lemma 4.3, we know that

$$|w(\eta)| \geq \frac{2}{P''_m(0)}$$

is necessary and sufficient. Since $T'_m(v_0)^2/(T_m(v_0)T''_m(v_0))$ is decreasing for $v_0 \geq 1$ (see Lemma A.1), we infer from the definition of η in (4.5) that

$$|w(\eta)| \geq 6 \frac{m^2}{m^2 - 1} = \frac{2T'_m(1)^2}{T_m(1)T''_m(1)} \geq \frac{2T'_m(v_0)^2}{T_m(v_0)T''_m(v_0)} = \frac{2}{P''_m(0)}. \quad \square$$

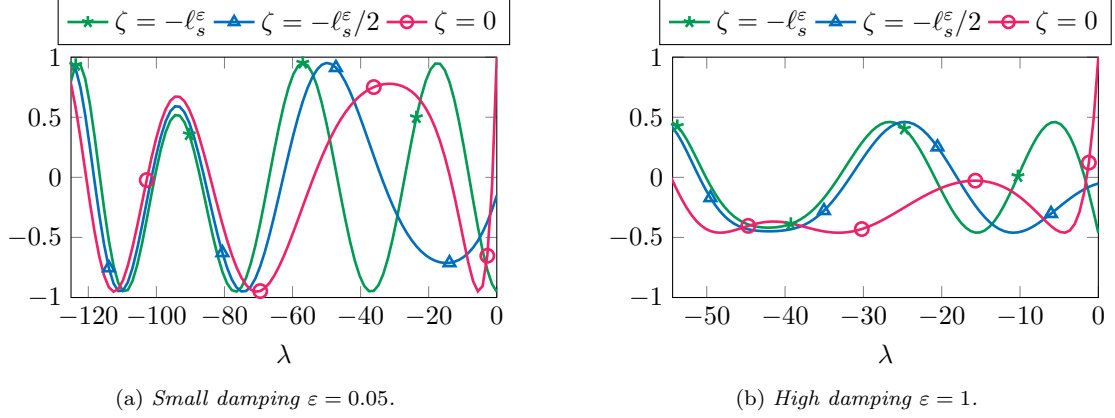


Figure 8. Stability polynomial $R_{s,m}(\lambda, \zeta, \tau, \eta)$ of the mRKC method vs. λ for $\zeta = -\ell_s^\varepsilon, -\ell_s^\varepsilon/2$ or 0 and $s = 5, m = 3, \tau = 1, \eta$ as in (4.5) and damping $\varepsilon = 0.05$ (left) or $\varepsilon = 1$ (right).

In the continuous setting in Section 2.3, η directly depends on f_S ; indeed, the condition $|\varphi(\eta\lambda)(\lambda + \zeta)| \leq |\zeta|$ implies $\eta \geq 2/|\zeta|$ (see Theorem 2.7). Therefore, η could rapidly grow as $\zeta \rightarrow 0$. In contrast, for the mRKC method, η depends only indirectly on f_S : η depends on the s -stage RKC method, which in turn depends on f_S . This indirect dependence of η on f_S creates a “protective buffer”, which prevents the explosion of η as $\zeta \rightarrow 0$; indeed, $\ell_s^\varepsilon \geq 2$ for all $s \in \mathbb{N}$.

The restriction $\varepsilon \leq \bar{\varepsilon}_m$ is necessary for proving Lemma 4.3, but probably not needed in practice. Indeed, we have verified numerically that for any $\varepsilon \geq 0$, $\Phi_m(z)(z + w) \in [w, 0]$ for all $z \in [-\ell_m^\varepsilon, 0]$ if, and only if, $|w| \geq 2/P_m''(0)$. Hence, we can suppose $\varepsilon_m = \varepsilon$ in (4.5) and replace $\ell_s^\varepsilon, \ell_m^\varepsilon$ by $\beta s^2, \beta m^2$, respectively, which yields (3.4). In Figure 8, we display the stability polynomial $R_{s,m}(\lambda, \zeta, \tau, \eta)$ for $s = 5$ and $m = 3$ as a function of λ for $\varepsilon = 0.05$ or $\varepsilon = 1$. Here, we set $\tau = 1, \eta$ to its lower bound in (4.5), and $\zeta = -\ell_s^\varepsilon, -\ell_s^\varepsilon/2$ or 0 . Since $|R_{s,m}(\lambda, \zeta, \tau, \eta)| \leq 1$, the mRKC method is always stable.

Stability analysis for a 2×2 model problem

Here, we consider a 2×2 linear model problem where the Jacobians of f_F and f_S are not simultaneously triangularizable. Then, the stability analysis cannot be reduced to the scalar multirate test equation (2.10), yet we shall show that the same stability conditions still hold. Moreover, we introduce a coupling term between the fast and slow variables and show that the same stability conditions are necessary even when the coupling is weak.

Thus, we consider the system of differential equations

$$y' = Ay, \quad \text{with} \quad A = \begin{pmatrix} \zeta & \sigma \\ \sigma & \lambda \end{pmatrix} \quad (4.6)$$

and $y(0) = y_0 \in \mathbb{R}^2$. We let $\lambda, \zeta < 0, \sigma \in \mathbb{R}$ the coupling term, and assume that $\sigma^2 \leq \lambda\zeta$ to ensure that both eigenvalues of A are negative or zero. We note $D \in \mathbb{R}^{2 \times 2}$ the diagonal matrix satisfying $D_{11} = 0$ and $D_{22} = 1$ and consider the splitting defined by $f_F(y) = A_F y$ and $f_S(y) = A_S y$, where

$$A_F := DA = \begin{pmatrix} 0 & 0 \\ \sigma & \lambda \end{pmatrix}, \quad A_S := (I - D)A = \begin{pmatrix} \zeta & \sigma \\ 0 & 0 \end{pmatrix}. \quad (4.7)$$

Observe that $\rho_F = |\lambda|$ and $\rho_S = |\zeta|$. The matrices A_F, A_S are simultaneously triangularizable if, and only if, they have a common eigenvector, which occurs only for $\sigma = 0$ or $\sigma^2 = \lambda\zeta$. We set $\sigma = 0.1\sqrt{\lambda\zeta}$, so that the present stability analysis cannot be reduced to the scalar multirate test equation (2.10). Furthermore, as the eigenvalues of A are negative or zero for all $|\sigma| \leq \sqrt{\lambda\zeta}$, the current coupling $\sigma = 0.1\sqrt{\lambda\zeta}$ can be considered to be weak when compared to the maximal coupling $\sqrt{\lambda\zeta}$.

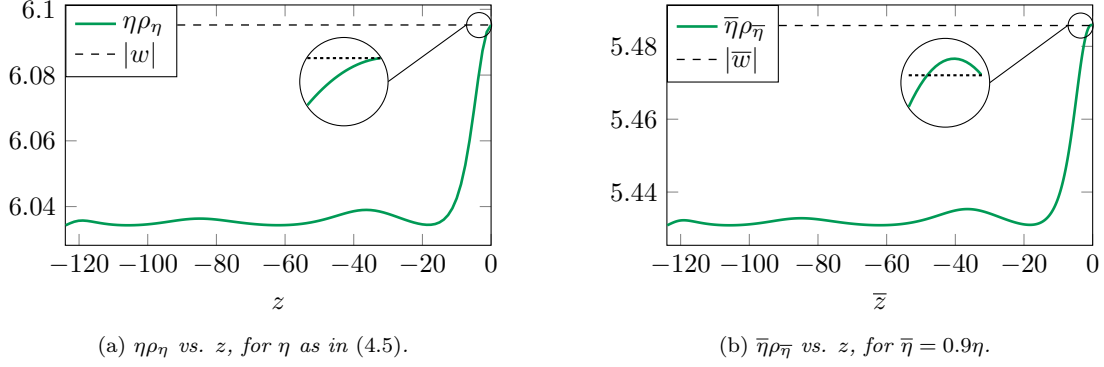


Figure 9. Verification that conditions (4.5) are sufficient and necessary for the stability of mRKC applied to the 2×2 test problem (4.6).

Given $y \in \mathbb{R}^2$, we obtain $\bar{f}_\eta(y)$ by replacing λ, ζ in (4.4) by A_F, A_S , respectively. This yields

$$\bar{f}_\eta(y) = A_\eta y, \quad \text{with} \quad A_\eta = \Phi_m(\eta A_F) A y, \quad (4.8)$$

and since Φ_m is a polynomial, A_η is well-defined. From (3.5) it follows $y_{n+1} = R_s(\tau A_\eta) y_n$. If the eigenvalues of τA_η are in the interval $[-\ell_s^\varepsilon, 0]$, the mRKC method is stable. For convenience, we set $\tau = 1$, $|\zeta| = \ell_s^\varepsilon$ with $s = 10$, and also fix $m = 8$ and $\eta = \frac{6\tau}{\ell_s^\varepsilon} \frac{m^2}{m^2-1}$ (as in (4.5)). Then, the mRKC method is stable if the spectral radius ρ_η of A_η satisfies $\rho_\eta \leq |\zeta|$ for all $\eta \lambda \in [-\ell_m^\varepsilon, 0]$, or equivalently $\eta \rho_\eta \leq \eta |\zeta| = |w|$.

In Figure 9(a), we display $\eta \rho_\eta$ as a function of $z = \eta \lambda \in [-\ell_m^\varepsilon, 0]$ and observe that $\eta \rho_\eta \leq |w|$; thus, the mRKC scheme is stable. Hence, the stability conditions (3.4) guarantee stability of the scheme even though the Jacobians of f_F, f_S are not simultaneously triangularizable.

Next, in Figure 9(b), we consider a value of η smaller than that dictated by (4.5). For $\bar{\eta} = 0.9\eta$, we again display $\bar{\eta} \rho_{\bar{\eta}}$ as a function of $\bar{z} = \bar{\eta} \lambda \in [-\ell_m^\varepsilon, 0]$. Then, a small region of instability appears for \bar{z} close to zero, where $\bar{\eta} \rho_{\bar{\eta}} > |\bar{w}|$. Hence, the stability conditions (4.5) are necessary even for systems of equations with a weak coupling $\sigma = 0.1\sqrt{\lambda\zeta}$, where $\sqrt{\lambda\zeta}$ corresponds to the maximal coupling strength. Similar instabilities as in Figure 9(b) occur for even weaker couplings $\sigma = 0.01\sqrt{\lambda\zeta}$, $\sigma = 0.001\sqrt{\lambda\zeta}$ and for larger $\bar{\eta} = 0.95\eta$.

4.2 Convergence analysis

We end this section by proving that the mRKC scheme is first-order accurate.

Theorem 4.6. *The mRKC scheme is first-order accurate.*

Proof. We estimate the local error after one step. From Definition 2.1 with y replaced by y_0 in (2.3) follows $u(\eta) = y_0 + \eta f(y_0) + \mathcal{O}(\eta^2)$ and thus $f_\eta(y_0) = f(y_0) + \mathcal{O}(\eta)$. Let $y(\tau)$ and $y_\eta(\tau)$ be the solutions of (1.1) and (2.1) at time τ , respectively, then

$$y(\tau) - y_\eta(\tau) = \tau(f(y_0) - f_\eta(y_0)) + \mathcal{O}(\tau^2) = \mathcal{O}(\eta\tau + \tau^2).$$

Let $\bar{y}_\eta(\tau)$ be the solution of $\bar{y}'_\eta = \bar{f}_\eta(\bar{y}_\eta)$ with $\bar{y}_\eta(0) = y_0$ and \bar{f}_η as in (3.6) and (3.7). Since the RKC scheme (3.7) is first-order accurate then $u_\eta = u(\eta) + \mathcal{O}(\eta^2)$ and $\bar{f}_\eta(y_0) = f_\eta(y_0) + \mathcal{O}(\eta)$, which yields

$$y_\eta(\tau) - \bar{y}_\eta(\tau) = \tau(f_\eta(y_0) - \bar{f}_\eta(y_0)) + \mathcal{O}(\tau^2) = \mathcal{O}(\eta\tau + \tau^2).$$

Finally, let y_1 be the solution after one step of the mRKC scheme (3.5) to (3.7), which can also be seen as the solution after one step of the RKC scheme applied to $\bar{y}'_\eta = \bar{f}_\eta(\bar{y}_\eta)$. Using the fact that the RKC scheme (3.5) has first-order accuracy then

$$\bar{y}_\eta(\tau) - y_1 = \mathcal{O}(\tau^2).$$

By triangular inequality we obtain $|y(\tau) - y_1| = \mathcal{O}(\eta\tau + \tau^2)$ and from (3.4) follows $\eta \leq 8\tau$, thus $|y(\tau) - y_1| = \mathcal{O}(\tau^2)$ and the scheme is first-order accurate. \square

Typically $s \gg 1$, i.e. $\eta \ll \tau$, and the error made when approximating f by the averaged force f_η is negligible. In fact, we observe that the difference between the RKC and the mRKC solutions in our numerical experiments in Section 5 is always very small.

5 Numerical Experiments

In this section we compare the mRKC scheme from Section 3.2 against the classical RKC method of Section 3.1 through a series of experiments. First, we apply mRKC to a stiff nonlinear dynamical system to verify convergence in the standard “ODE sense” and underpin its efficiency. Then, we apply mRKC to the heat equation and verify convergence in the “PDE sense”, i.e. when both the mesh size H and the time step τ decrease simultaneously. In the third experiment, we compare the performance and efficiency of the mRKC and RKC schemes when applied to a linear diffusion problem in complex geometry; here, we also compare mRKC to a second-order accurate RKC scheme (RKC2) [54, 64] and the implicit Euler method. In the fourth experiment, we apply the mRKC scheme with the RKC, RKC2 and the implicit Euler method to a nonlinear integro-differential problem. Finally, we study numerically the stability of mRKC when it is applied to various advection-diffusion-reaction problems.

Both the RKC and mRKC methods need bounds on the spectral radii of the Jacobians of f_F and f_S to determine the number of stages s, m needed for stability. In our experiments, we estimate them with a cheap nonlinear power method [38, 62]. The numerical experiments in Sections 5.2, 5.3 and 5.5 were performed using the C++ library `libMesh` [33], while for the experiments of Sections 5.1 and 5.4 we used the `Eigen` library [22].

5.1 Robertson’s stiff test problem

First, we study the convergence of the mRKC scheme on a popular stiff test problem, Robertson’s nonlinear chemical reaction model [15, 29]:

$$\begin{aligned} y_1' &= -0.04 y_1 + 10^4 y_2 y_3, & y_1(0) &= 1, \\ y_2' &= 0.04 y_1 - 10^4 y_2 y_3 - 3 \cdot 10^7 y_2^2, & y_2(0) &= 2 \cdot 10^{-5}, \\ y_3' &= 3 \cdot 10^7 y_2^2, & y_3(0) &= 10^{-1}, \end{aligned} \quad (5.1)$$

where $t \in [0, 100]$. With this set of parameters and initial conditions, the only term inducing severe stiffness is $-10^4 y_2 y_3$. Thus, we let

$$f_F(y) = \begin{pmatrix} 0 \\ -10^4 y_2 y_3 \\ 0 \end{pmatrix}, \quad f_S(y) = \begin{pmatrix} -0.04 y_1 + 10^4 y_2 y_3 \\ 0.04 y_1 - 3 \cdot 10^7 y_2^2 \\ 3 \cdot 10^7 y_2^2 \end{pmatrix}, \quad f(y) = f_F(y) + f_S(y).$$

Now, we solve (5.1) either with the RKC or the mRKC scheme using step sizes $\tau = 1/2^k$, $k = 0, \dots, 7$. For comparison, we use a reference solution obtained with the standard fourth-order Runge–Kutta scheme using $\tau = 10^{-4}$. In Figure 10(a), we observe that both the RKC and the mRKC method achieve first-order convergence. In fact, both errors are hardly distinguishable, indicating that the error introduced by the approximation of f by f_η is negligible. We observe in Figure 10(b) that the mean value of η during integration is indeed considerably smaller than τ .

Next, we compare the two schemes for a fixed step size $\tau = 1$. In Figure 11(a), we display the number of stages taken by the mRKC and the RKC method at each time step with respect to $t \in [0, 100]$. Moreover, Figure 11(b) depicts the evolution of the spectral radii ρ, ρ_F, ρ_S of the Jacobians of f, f_F, f_S , respectively. We observe that ρ_S decreases with time and consequently the mRKC scheme decreases the number s of expensive function evaluations f_S per step. In contrast, ρ increases and thus the RKC scheme must increase the number s of f_S function evaluations, although

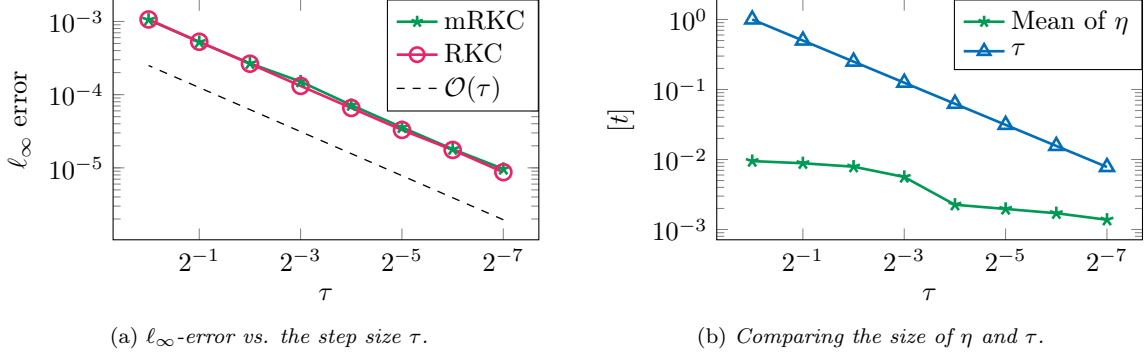


Figure 10. Robertson's stiff test problem. Convergence and comparison of η against τ .

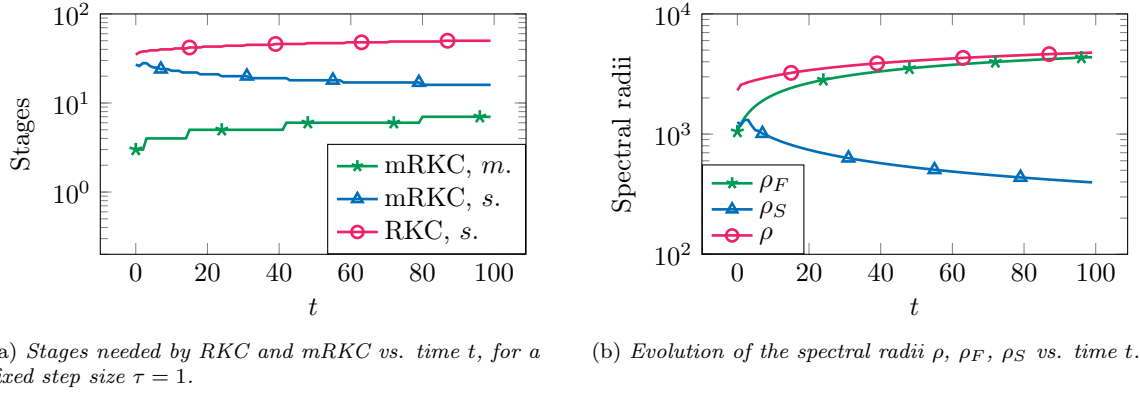


Figure 11. Robertson's stiff test problem. Comparison of spectral radii and number of stages taken by the mRKC and the RKC scheme.

this term does not introduce any stiffness; indeed, ρ increases only because of the term contained in f_F . Finally, we notice in Figure 11(a) that the mRKC scheme increases the number m of (cheap) function evaluations f_F because of the increase in ρ_F and η ; indeed, η also increases due to the decrease in s and (3.4). This added cost, however, is much smaller than that from the many additional (expensive) evaluations of f_S required by the RKC method.

5.2 Heat equation in the unit square

Next, we verify the space-time convergence properties of the mRKC method. To do so, we consider the heat equation in the unit square $\Omega = [0, 1] \times [0, 1]$,

$$\begin{aligned} \partial_t u - \Delta u &= g && \text{in } \Omega \times [0, T], \\ u &= 0 && \text{in } \partial\Omega \times [0, T], \\ u &= 0 && \text{in } \Omega \times \{0\}, \end{aligned} \quad (5.2)$$

where $T = 1/2$ and g is chosen such that $u(\mathbf{x}, t) = \sin(\pi x_1)^2 \sin(\pi x_2)^2 \sin(\pi t)^2$ is the exact solution.

Starting from a mesh of $2^j \times 2^j$ simplicial elements with $j = 2, \dots, 5$, we locally refine twice all the elements inside the square $\Omega_F = (1/4, 3/4) \times (1/4, 3/4)$. Each refinement step is performed by splitting all edges of any simplex, i.e. every triangle is split into four self-similar children. Let \mathcal{M} be the set of elements in the mesh and $\mathcal{M}_F = \{T \in \mathcal{M} : \bar{T} \cap \Omega_F \neq \emptyset\}$ the set of refined elements or their direct neighbors. Then $h = H/4$ is the diameter of the elements inside of Ω_F , with H the diameter of the elements outside of Ω_F .

Next, we discretize (5.2) in space with first-order DG-FE [10] on the mesh \mathcal{M} . After inverting

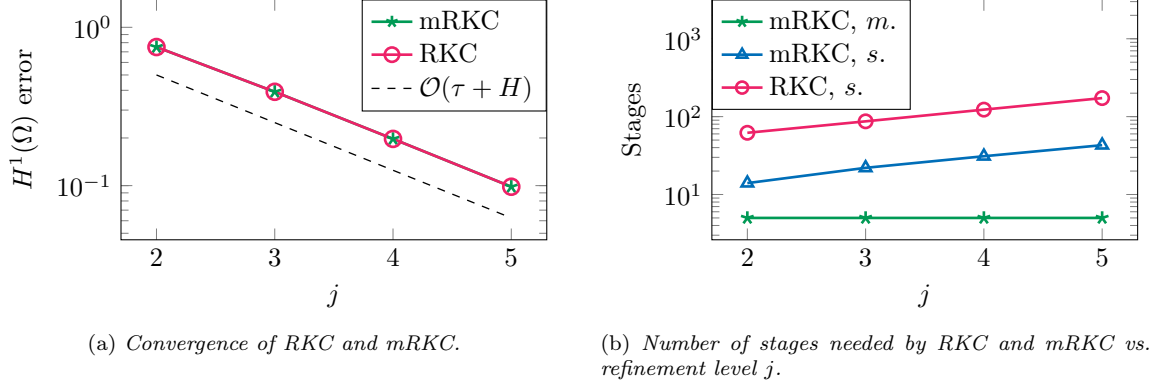


Figure 12. Heat equation in the unit square. Space-time convergence and number of stages.

the block-diagonal mass matrix, the resulting system is

$$y' = Ay + G, \quad y(0) = y_0,$$

where $A \in \mathbb{R}^{N \times N}$ and $G \in C([0, T], \mathbb{R}^N)$ corresponds to the spatial discretization of $g(\cdot, t)$. Let $D \in \mathbb{R}^{N \times N}$ be a diagonal matrix with $D_{ii} = 1$ if the i th degree of freedom belongs to an element in \mathcal{M}_F and $D_{ii} = 0$ otherwise. We also introduce

$$A_F = DA, \quad A_S = (I - D)A \quad \text{and} \quad f_F(y) = A_F y, \quad f_S(t, y) = A_S y + G(t), \quad (5.3)$$

with I the identity. It is well-known that the spectral radii ρ_S and ρ_F of A_S and A_F behave as $\mathcal{O}(1/H^2)$ and $\mathcal{O}(1/h^2) = \mathcal{O}(16/H^2)$, respectively.

We now consider a sequence of meshes with $j = 2, \dots, 5$ and solve (5.2) either with the mRKC or the RKC scheme using the same step size $\tau = 1/2^j$. The parameters s and m for mRKC are chosen according to (3.13). In Figure 12(a), we display the $H^1(\Omega)$ errors at final time for mRKC and RKC. Both methods yield space-time first-order convergence and result in similar errors. In Figure 12(b), we show the number of stages needed by RKC and mRKC. For both schemes, s increases as the mesh size H decreases, but for mRKC, s is much smaller, since it only depends on the coarse elements, while m remains constant due to the constant ratio between ρ_F and ρ_S .

5.3 Diffusion across a narrow channel

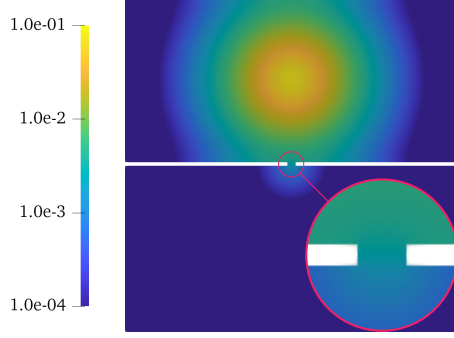
To illustrate the efficiency of the mRKC method in a situation where geometry constraints require local mesh refinement, we consider the heat equation

$$\begin{aligned} \partial_t u - \Delta u &= g & \text{in } \Omega_\delta \times [0, T], \\ \nabla u \cdot \mathbf{n} &= 0 & \text{in } \partial\Omega_\delta \times [0, T], \\ u &= 0 & \text{in } \Omega_\delta \times \{0\}, \end{aligned} \quad (5.4)$$

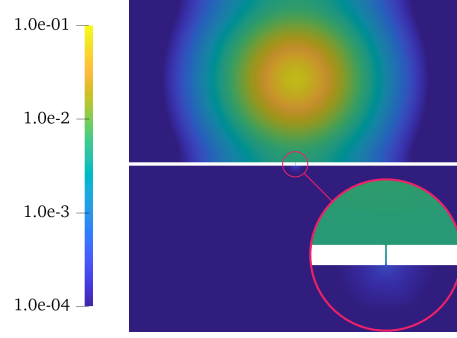
with $T = 0.1$ inside Ω_δ , which consists of two 10×5 rectangles linked by a narrow $\delta \times 0.05$ channel of width $\delta > 0$, see Figure 13. The right-hand side $g(\mathbf{x}, t) = \sin(10\pi t)^2 e^{-5\|\mathbf{x} - \mathbf{c}\|^2}$ corresponds to a smoothed Gaussian point source centered at \mathbf{c} in the middle of the upper rectangle.

Inside Ω_δ , we use a Delaunay triangulation with maximal element size $H \approx 0.015$. As δ approaches zero, the elements inside the channel become increasingly smaller and the system stiffer. For each $\delta > 0$, we define a neighborhood $\Omega_{F,\delta} \subset \Omega_\delta$ of the channel and \mathcal{M}_F , A , A_F , A_S , f_F , f_S as in Section 5.2. Here, $\Omega_{F,\delta}$ is chosen such that the spectral radius of A_S is almost independent of δ and only that of A_F increases with decreasing δ . Hence, $\Omega_{F,\delta}$ contains the channel together with all neighboring elements of mesh size smaller than H , see Figures 14(a) and 14(b).

For varying channel width $\delta = 1/2^k$, $k = 0, \dots, 15$, we now solve (5.4) with the RKC and mRKC method using the choice of parameters (3.13) with $\tau = 0.01$. In Figure 15(a), the relative speed-up

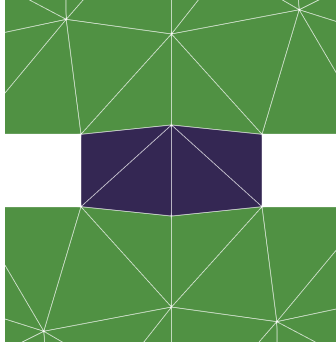


(a) Solution for $\delta = 1/2^2$.

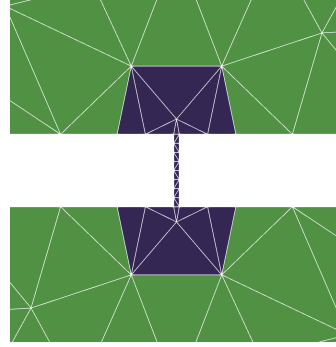


(b) Solution for $\delta = 1/2^7$.

Figure 13. *Narrow channel. Numerical solutions of (5.4) at $t = 1$ using mRKC for a channel width $\delta = 1/2^2$ or $\delta = 1/2^7$.*



(a) Zoom over the channel with $\delta = 1/2^2$.



(b) Zoom over the channel with $\delta = 1/2^7$.

Figure 14. *Narrow channel. Zoom of the FE mesh for a channel width $\delta = 1/2^2$ or $1/2^7$, with the subdomain $\Omega_{F,\delta}$ (in blue).*

defined as the ratio between the computational times of RKC and mRKC always exceeds one and reaches a value as high as 40. Note that the relative error between the two solutions in $L^2(\Omega_\delta)$ or $H^1(\Omega_\delta)$ norm is at most $3 \cdot 10^{-4}$, as shown in Figure 15(c).

In Figure 15(d), we display for varying δ also the spectral radii ρ, ρ_F, ρ_S of A, A_F, A_S , respectively; note that ρ_F and ρ essentially coincide. For large δ , we also have $\rho_F \approx \rho_S$ since the typical element size is sufficiently small to resolve the channel (Figure 14(a)). For δ small, we observe that ρ, ρ_F increase as $1/\delta^2$ while ρ_S remains almost constant. Figure 15(e) shows that the number s of stages in the mRKC scheme remains constant, as does ρ_S in Figure 15(d), while m increases (as ρ_F). For large δ , we have $\rho_F \approx \rho_S$ and thus $m = 1$; then, the RKC and mRKC schemes coincide. Indeed, as is shown in Figure 15(c), for $m = 1$ then the relative error between the RKC and mRKC solutions is of the order of machine precision.

In Figure 15(b), we observe that for δ large the CPU times of the two methods are similar; thus, despite $\rho_F \approx \rho_S$, there is no loss in efficiency and the speed-up is at least one (Figure 15(a)). For moderate values of δ , the cost of RKC increases proportionally to $1/\delta$, while the cost of mRKC is hardly affected. For even smaller δ , the number of evaluations of f_F increases and so does its cost with respect to f_S (see Figure 15(f)), since the number of elements in \mathcal{M}_F increases (Figure 14). In this regime, evaluation of f_F dominates the computational cost of mRKC, which increases linearly in $1/\delta$, too. Still, the mRKC method remains about forty times faster than the classical RKC method for this particular discretization inside Ω_δ , see Figure 15(a).

Finally, we compare mRKC against the second-order accurate version of the RKC scheme (RKC2) from [54, 64] and the implicit Euler (IE) method. To do so, we consider the two channel widths $\delta = 1/2^6, 1/2^{12}$ and solve (5.4) with the RKC, RKC2, mRKC and IE schemes. For both values of δ we display in Figure 16 the computational times against the final error, with varying step size $\tau = T/2^j$, $j = 0, \dots, 16$ and $T = 0.1$. Since the exact solution is unknown, the final error is computed against a reference solution obtained from the second-order RKC2 scheme with step size $\tau = 10^{-6}$. For the wider channel with $\delta = 1/2^6$, we observe in Figure 16(a) that the mRKC scheme is more efficient than RKC2 for most of the step sizes, but becomes less efficient at higher accuracy. The IE and the mRKC method are about equally efficient. In contrast, for the narrow channel with $\delta = 1/2^{12}$, that is, in a situation of even more severe stiffness, we observe in Figure 16(b) that mRKC is always much faster than RKC2: the speed-up ranges from ten to seventy times faster, depending on the step size imposed by the desired accuracy. In this case of extreme stiffness, the IE method always remains slightly faster than mRKC; clearly, the IE method is also particularly efficient here thanks to the symmetry and linearity of the discrete Laplacian.

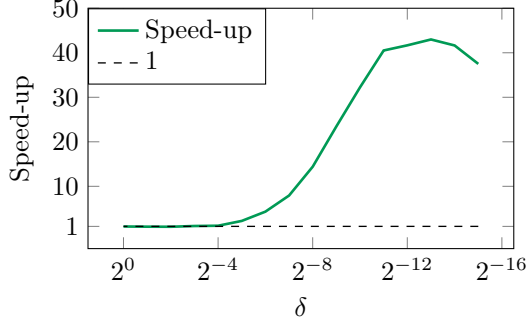
5.4 Integro-differential equation

To compare the mRKC and implicit Euler scheme on a nonsymmetric and truly nonlinear problem, we now consider the one-dimensional integro-differential problem from [61], also considered in [6, 66]:

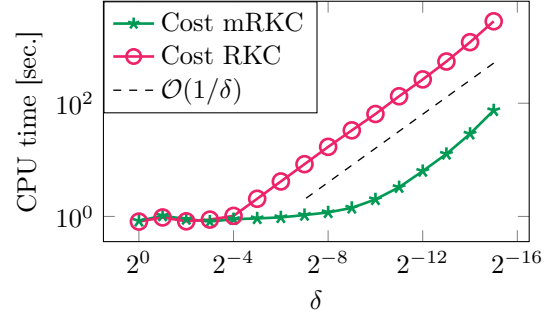
$$\begin{aligned} \partial_t u(t, x) &= \Delta u(t, x) - \sigma \int_0^1 \frac{u(t, s)^4}{(1 + |x - s|)^2} ds & (t, x) &\in [0, 1] \times [0, 1], \\ u(0, x) &= \cos(x\pi/2)^2 & x &\in [0, 1], \\ u(t, 0) &= 1 - \sqrt{t}/2 & t &\in [0, 1], \\ \partial_x u(t, 1) &= 0 & t &\in [0, 1], \end{aligned} \tag{5.5}$$

with $\sigma = 0.01$. Problem (5.5) models an idealized temperature profile of air near the ground. We discretize (5.5) in space on a uniform grid of N cells using central finite differences for the Laplacian and the composite trapezoidal rule for the integral term. For the mRKC scheme, we assign the Laplacian to f_F and the integral term to f_S . For the implicit Euler method, the Jacobian (evaluated analytically) and its QR decomposition are computed only once per time step following [29, IV.8].

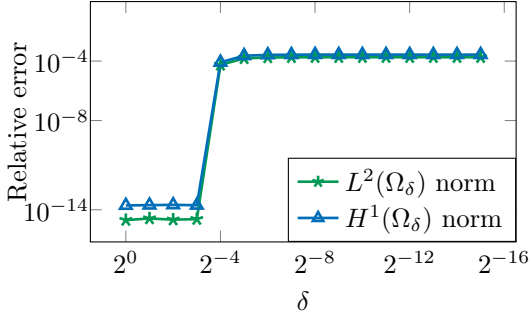
For $N = 100, 3200$ (varying problem size and degree of stiffness), we apply the RKC, RKC2, mRKC and IE schemes for $\tau = 1/2^j$ with $j = 2, \dots, 12$. For each run, we monitor the computational time and the $L^2([0, 1])$ error against a reference solution: the resulting efficiency graphs are shown in Figure 17. For $N = 100$, IE method is always faster than RKC, which remains the most expensive



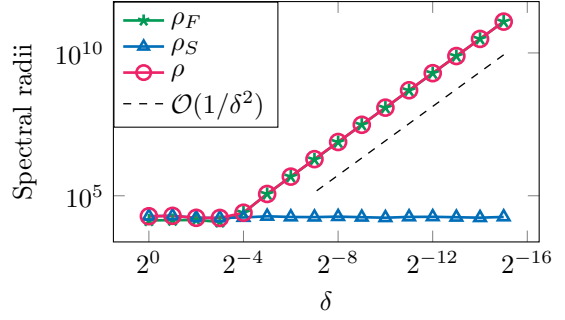
(a) Relative speed-up of mRKC over RKC.



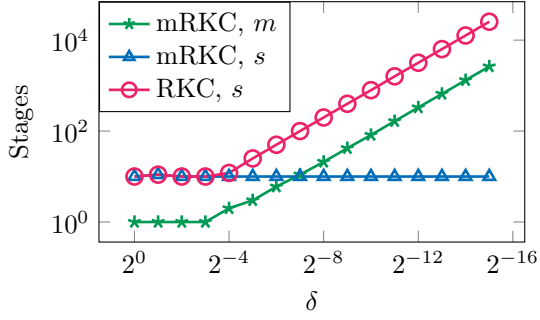
(b) Total CPU time w.r.t. δ .



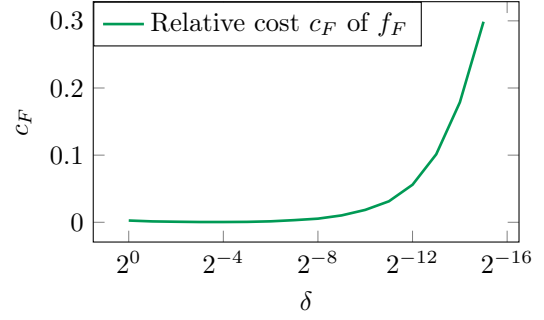
(c) RKC and mRKC solutions' relative error $\|u^{\text{mRKC}} - u^{\text{RKC}}\|/\|u^{\text{RKC}}\|$.



(d) Spectral radii w.r.t. δ .



(e) Number of stages needed by RKC and mRKC.



(f) Relative evaluation cost of $f_F(y)$ w.r.t. $f_F + f_S$ as a function of δ .

Figure 15. Narrow channel. Speed-up, error, spectral radii and stages number w.r.t. channel width δ .

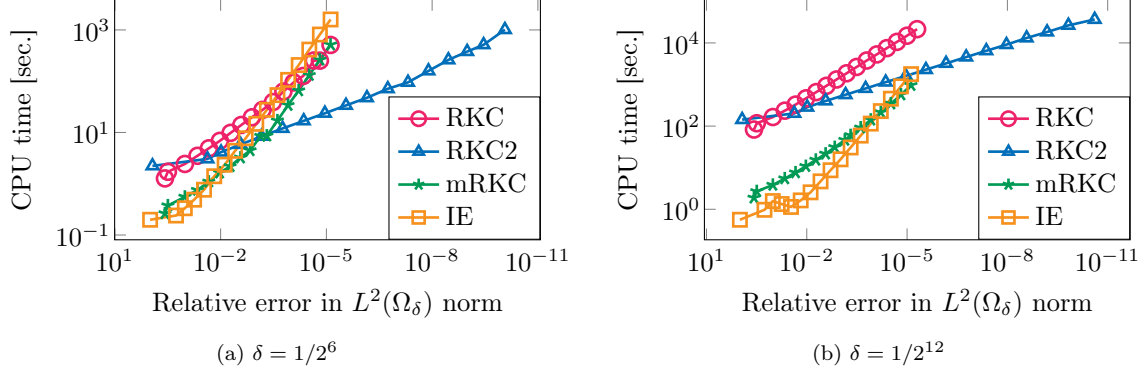


Figure 16. *Narrow channel. Work vs. accuracy diagram of the RKC, RKC2, mRKC and implicit Euler (IE) scheme for two channel widths δ . Symbols represent step sizes $\tau = T/2^j$, for $j = 0, \dots, 16$.*

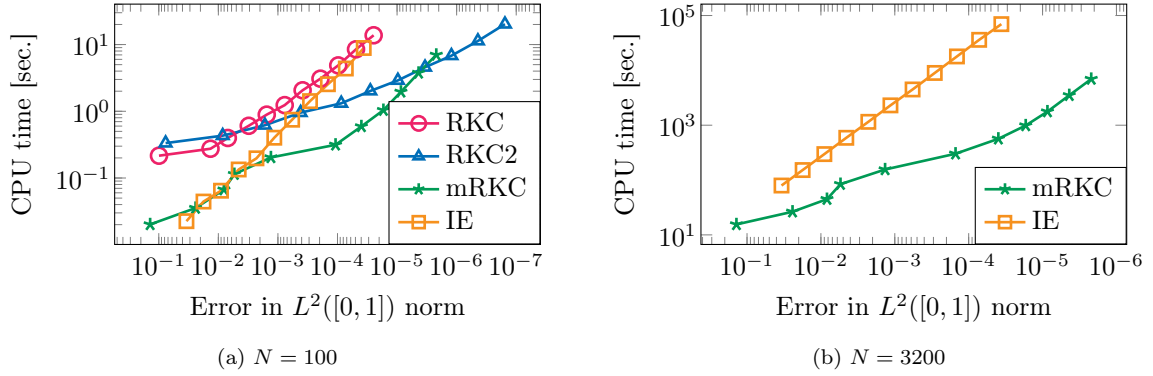


Figure 17. *Integro-differential problem. Work vs. accuracy diagram of the RKC, RKC2, mRKC and implicit Euler (IE) scheme for two mesh sizes $1/N$. Symbols represent step sizes $\tau = 1/2^j$, for $j = 2, \dots, 12$.*

method. For large τ , IE is comparable to mRKC, but as τ decreases, the mRKC scheme becomes significantly more efficient. The second-order scheme RKC2 becomes faster than mRKC only at high accuracy. For the stiffer case with $N = 3200$, the mRKC scheme is the fastest method, as its efficiency is only marginally affected by the increased stiffness, while the cost of the direct solver in the Newton iteration clearly starts to dominate the overall cost of IE. For those parameter settings, the RKC and RKC2 methods were overly expensive and could not be run to completion.

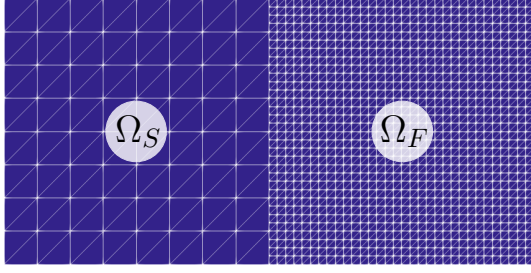
5.5 Reaction-convection-diffusion problem

In Section 4.1 we proved that the stability conditions of the mRKC method are the same for the 2×2 model problem (4.6) and for the scalar multirate test equation (2.10). The splitting of the discrete Laplace operator in (5.3) in fact is similar to that in (4.7) for the 2×2 model problem. Thus, one could expect that the stability conditions (3.4) are also necessary for more general parabolic problems. However, spatial discretizations of parabolic problems are much more complex than (4.6). Here we shall demonstrate via numerical experiment that the weaker stability conditions (3.13) in fact are also necessary and sufficient for general parabolic reaction-convection-diffusion problems, such as

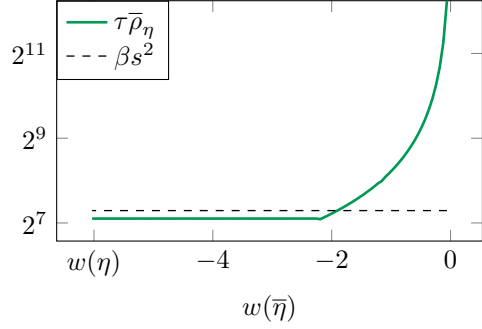
$$\begin{aligned} \partial_t u - \nabla \cdot (K \nabla u) + \beta \cdot \nabla u + \mu u &= g && \text{in } \Omega \times [0, T], \\ u &= 0 && \text{in } \partial\Omega \times [0, T], \\ u &= u_0 && \text{in } \Omega \times \{0\}. \end{aligned}$$

These experiments also illustrate that the mRKC method indeed requires no scale separation.

We now consider three distinct parameter regimes. First, we let $\Omega = [0, 2] \times [0, 1]$, $K = I_{2 \times 2}$, $\beta = \mathbf{0}$ and $\mu = 0$. Inside Ω , we build a 16×8 uniform mesh and refine twice the elements inside of



(a) Domains Ω_S and Ω_F



(b) $\tau\bar{\rho}_\eta$ vs. $w(\bar{\eta})$, first problem.

Figure 18. Reaction-convection-diffusion problem. Mesh and spectral radius $\tau\bar{\rho}_\eta$ of the first problem setting.

$\Omega_F = (1, 2) \times (0, 1)$ (see Figure 18(a)). Again, we use DG-FE for the spatial discretization, which yields the two matrices A_F and A_S , as described in Section 5.2. Next, we set $\tau = 1$, s, m, η as in (3.4) and A_η as in (4.8). One step of the mRKC scheme is given by $y_1 = R_s(\tau A_\eta)y_0$. We recall that a necessary condition for stability of the scheme (at least for linear problems) is $\tau\rho_\eta \leq \beta s^2$, where ρ_η is the spectral radius of A_η .

Let $\bar{\beta}$ be as in (3.13), $\bar{\eta} \in [0, \eta]$, \bar{m} such that $\bar{\eta}\rho_F \leq \bar{\beta}\bar{m}^2$,

$$\bar{A}_\eta = \Phi_{\bar{m}}(\bar{\eta}A_F)A$$

and $\bar{\rho}_\eta$ be the spectral radius of \bar{A}_η . We wish to study for which $\bar{\eta}$ it holds $\tau\bar{\rho}_\eta \leq \beta s^2$. In Figure 18(b), we display $\tau\bar{\rho}_\eta$ for $\bar{\eta} \in (0, \eta)$ with respect to $w(\bar{\eta}) = -\bar{\eta}\beta s^2/\tau$: for $|w(\bar{\eta})| \geq 2$, it holds $\tau\bar{\rho}_\eta \leq \beta s^2$ and thus the scheme is stable. Observe that $|w(\bar{\eta})| \geq 2$ is equivalent to $\bar{\eta} \geq 2\tau/(\beta s^2)$, as in (3.13). Since the smallest (in magnitude) nonzero eigenvalues of the discrete Laplacians, A_F and A_S , do not depend on the mesh size, but only depends on the size of the domain, they essentially coincide; hence, this problem exhibits no scale separation assumption. Nevertheless the mRKC scheme remains stable, as expected from theory.

Finally, we consider two additional cases that further corroborate the previous findings. First, we set $\Omega = [0, 1] \times [0, 1]$, $K = I_{2 \times 2}$, $\beta = (1, 1)^\top$ and $\mu = 1$. In Ω , we build a 8×8 uniform mesh and refine three times the elements inside the small inner square $\Omega_F = (1/4, 3/4) \times (1/4, 3/4)$. In Figure 19(a), we show again $\tau\bar{\rho}_\eta$ for $\bar{\eta} \in (0, \eta)$ with respect to $w(\bar{\eta})$: for $|w(\bar{\eta})| \geq 2$, $\tau\bar{\rho}_\eta \leq \beta s^2$ holds. Next, we use a uniform 32×32 mesh in $\Omega = [0, 1] \times [0, 1]$ which is refined twice in the lower left corner $\Omega_F = (0, 1/32) \times (0, 1/32)$. We also set $\beta = 0$, $\mu = 0$, $K(\mathbf{x}) = 1$ for $x_1 \geq x_2$ and $K(\mathbf{x}) = 0.1$ elsewhere. The results, shown in Figure 19(b), again confirm the stability of the mRKC with parameters chosen according to (3.13).

6 Conclusion

Starting from the stiff differential equation $y' = f_S(y) + f_F(y)$, where f_F represents a few severely stiff, but cheap, “fast” components, we have proposed a modified equation (2.1) whose stiffness no longer depends on f_F . It involves an averaged force f_η of $f = f_S + f_F$, evaluated by solving the stiff, but cheap, auxiliary problem (2.3) over short time and thus forms the basis of the following multirate strategy: Solve (2.1) with an explicit numerical method whose stability conditions are determined by the mildly stiff, but expensive, “slow” components f_S , while solving (2.3) with a separate explicit method whose stability conditions are determined by f_F , whenever an evaluation of f_η is needed. In Theorems 2.4 and 2.5, we have proved that the modified equation (2.1) approximates the original problem to first-order accuracy while preserving its contractivity properties. The stability analysis of the multirate test equation (2.13) underpins the reduced stiffness of the modified equation, which no longer depends on the fastest components f_F for η sufficiently large – see Theorem 2.7.

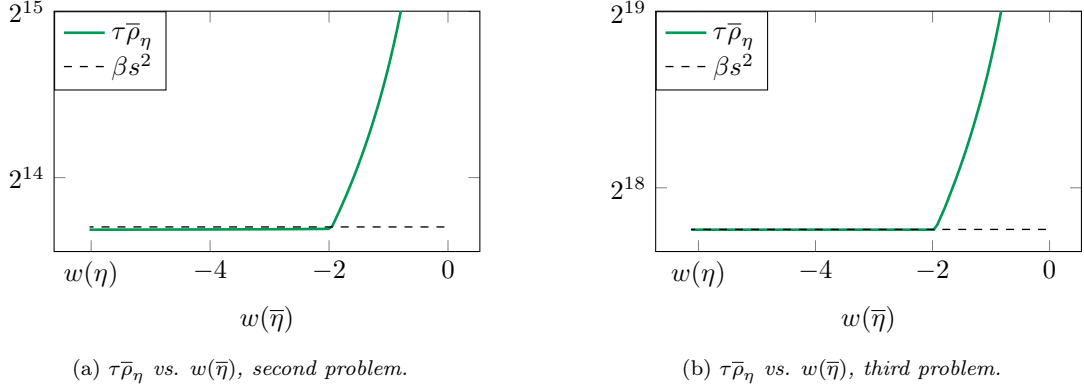


Figure 19. *Stability experiment. Illustration of $\tau\bar{\rho}_\eta$ versus $w(\bar{\eta})$, second and third problem setting.*

By discretizing (2.1) with an s -stage (explicit) Runge-Kutta-Chebyshev (RKC) method while evaluating f_η with one step of a separate m -stage RKC method, we have devised a new multirate RKC method. The resulting mRKC method, given by (3.4)–(3.7), is fully explicit, stable, and first-order accurate, as proved in Theorems 4.5 and 4.6, without the need for interpolation or extrapolation of missing stage values. Thanks to the reduced stiffness in (2.1), the number of expensive f_S evaluations is greatly reduced and independent of the severe stiffness induced by just a few degrees of freedom in f_F , without any assumption about scale separation.

For semi-discrete parabolic problems, where f_S and f_F correspond to discretized diffusion operators in the coarse and locally refined regions of the mesh, respectively, the mRKC method permits to overcome the crippling effect on explicit time integrators due to a few tiny elements or grid cells. In particular, for diffusion dominated problems in complex geometry, the mRKC method is up to forty times faster than a standard first-order RKC method; it is also up to seventy times cheaper than a second-order RKC2 [54, 64] method for moderately high error tolerances. Thus, the mRKC method recovers the well-known efficiency of RKC methods for large-scale, possibly nonlinear, parabolic problems without sacrificing explicitness, even in the presence of local mesh refinement. When compared to the implicit Euler method, the mRKC scheme’s performance depends on the degree of stiffness, problem size and nonlinearity. In all our numerical experiments, mRKC performed similarly, or even better, than IE, without the need for solving any linear systems. Moreover, our numerical experiments suggest that with increasing problem size, the efficiency of IE rapidly decreases, whereas mRKC remains only marginally affected.

The multirate strategy introduced here also paves the way for higher order extensions and for developing explicit stabilized multirate methods for stiff stochastic differential equations [4].

Acknowledgments

This research is partially supported by the Swiss National Science Foundation, grant no. 20020_172710. The second author thanks the EPFL for the opportunity to perform this research there during his sabbatical leave.

A Proofs of lemmas

In this section we prove Lemmas 4.3 and A.1, needed in the proof of Theorem 4.5.

Proof of Lemma 4.3. For the only if part we follow the lines of the proof of Lemma 2.6 and find that $\Phi'_m(0)|w| \geq 1$ is a necessary condition. The identity $\Phi'_m(0) = P''_m(0)/2$ follows from the definition of $\Phi_m(z)$ in (4.3).

Now, let us suppose $2/P''_m(0) \leq |w|$ and show $\beta_\varepsilon(z) = \Phi_m(z)(z+w) \geq w$, where ε is the damping. For $z = 0$ it is clear, independently of ε . We will show $\beta_0(z) > w$ for all $z < 0$, since $\beta_\varepsilon(z)$ depends

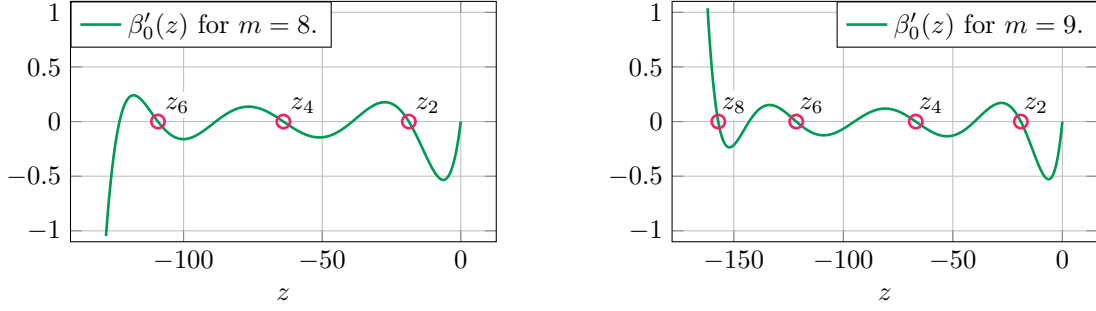


Figure 20. Plot of $\beta'_0(z)$ for $m = 8, 9$ and $|w| = 2/P''_m(0)$.

continuously on ε there exists $\varepsilon_m > 0$ such that $\beta_\varepsilon(z) \geq w$ for all $\varepsilon \leq \varepsilon_m$. We have

$$\begin{aligned}\beta'_0(z) &= \frac{P'_m(z)}{z}(z+w) - \frac{P_m(z)-1}{z^2}w, \\ \beta''_0(z) &= \frac{P''_m(z)}{z}(z+w) - 2\frac{P'_m(z)}{z^2}w + 2\frac{P_m(z)-1}{z^3}w\end{aligned}$$

and since $\beta_0(z)$ is a polynomial of degree m then $\beta'_0(z)$ has at most $m-1$ zeros. We are going to locate the zeros $z_{m-1} < \dots < z_3 < z_2$ of $\beta'_0(z)$. Then we will use the fact that $\beta'_0(z)$ has at most one zero on the right of z_2 . In order to help the understanding of the proof we plot $\beta'_0(z)$ in Figure 20 for two values of m .

Since $P_m(z) = T_m(1+z/m^2)$ and $T_m(\cos(\theta)) = \cos(m\theta)$, choosing z_{2k} such that

$$1 + \frac{z_{2k}}{m^2} = \cos(\theta_{2k}) \quad \text{with} \quad \theta_{2k} = \frac{2k\pi}{m}$$

it yields

$$\beta'_0(z_{2k}) = 0 \quad \text{for} \quad 2k = 2, 4, \dots, 2\lfloor \frac{m-1}{2} \rfloor.$$

Since z_{2k} is a local maximum of $P_m(z)$ then $P''_m(z_{2k}) < 0$ and $\beta''_0(z_{2k}) < 0$. In a neighborhood of z_{2k} we have

$$\beta'_0(z) = \beta''_0(z_{2k})(z - z_{2k}) + \mathcal{O}((z - z_{2k})^2),$$

hence for $\delta > 0$ small and $2k = 2, 4, \dots, 2(\lfloor \frac{m-1}{2} \rfloor - 1)$ we have $\beta'_0(z_{2k+2} + \delta) < 0$ and $\beta'_0(z_{2k} - \delta) > 0$, implying that there exists $z_{2k+1} \in [z_{2k+2}, z_{2k}]$ such that $\beta'_0(z_{2k+1}) = 0$. If m is odd then $2\lfloor \frac{m-1}{2} \rfloor = m-1$ and we located the zeros z_j for $j = 2, 3, \dots, m-1$. If m is even then $2\lfloor \frac{m-1}{2} \rfloor = m-2$, but $P_m(-2m^2) = 1$ and $P'_m(-2m^2) = -1$ and hence $\beta'_0(-2m^2) < 0$. Thus, since $\beta'_0(z_{m-2} - \delta) > 0$ there exists $z_{m-1} \in [-2m^2, z_{m-2}]$ such that $\beta'_0(z_{m-1}) = 0$. Finally, we located z_j for $j = 2, 3, \dots, m-1$ for m even and odd. We will show $\beta_0(z) > w$ for $z \in [z_2, 0[$ and then for $z \in [-2m^2, z_2]$.

Let $z \in [z_2, 0[$, if $z = z_1$ then $\beta'_0(z) = 0$ and else $\beta'_0(z) < 0$. Indeed, for z close to zero we have

$$\beta'_0(z) = 1 + \frac{1}{2}P''_m(0)w + (P''_m(0) + \frac{1}{3}P'''_m(0)w)z + \mathcal{O}(z^2).$$

If $2/P''_m(0) < |w|$ then $1 + \frac{1}{2}P''_m(0)w < 0$ and $\beta'_0(z) < 0$ in the neighborhood of zero. If $2/P''_m(0) = |w|$ then

$$\beta'_0(z) = \left(P''_m(0) - \frac{2}{3}\frac{P'''_m(0)}{P''_m(0)}\right)z + \mathcal{O}(z^2) = \frac{m^2+1}{5m^2}z + \mathcal{O}(z^2),$$

and $\beta'_0(z) < 0$ in the neighborhood of zero as well. If there exists $\bar{z} \in]z_2, 0[$ such that $\beta'_0(\bar{z}) > 0$ we can take $\delta > 0$ small enough to have $\bar{z} \in]z_2 + \delta, -\delta[$ and $\beta'_0(z_2 + \delta) < 0$ and $\beta'_0(-\delta) < 0$. Hence, β'_0 would change sign twice in the interval $]z_2 + \delta, -\delta[$, which is impossible since β'_0 has at most one zero on the right of z_2 . Hence, $\beta'_0(z) < 0$ for all $z \in [z_2, 0[$ except at most one point, since $\beta_0(0) = w$ it follows $\beta_0(z) > w$ for all $z \in [z_2, 0[$.

We consider now $z \leq z_2$. Using $1 - \cos(\theta) = 2 \sin(\theta/2)^2$ it holds $z_2 = -2m^2 \sin(\pi/m)$ and

$$\begin{aligned} \beta_0(z) &= \Phi_m(z)(z+w) = \frac{P_m(z)-1}{z}(z+w) \geq -2\frac{z+w}{z} \geq -2 - 2\frac{w}{z} \geq wP_m''(0) - 2\frac{w}{z_2} \\ &= \left(\frac{m^2-1}{3m^2} + \frac{1}{m^2 \sin(\pi/m)^2} \right) w > \left(\frac{1}{3} + \frac{1}{m^2 \sin(\pi/m)^2} \right) w. \end{aligned}$$

Thus, if $m^2 \sin(\pi/m)^2 \geq 3/2$ then $\beta_0(z) > w$. For $m = 2$ it is clearly true. We let $g(x) = x^2 \sin(\pi/x)^2$ and show that $g(x)$ is strictly increasing in $x \in [2, \infty[$, which implies $m^2 \sin(\pi/m)^2 \geq 3/2$ for all $m \geq 2$. We have

$$g'(x) = 2 \sin(\pi/x)(x \sin(\pi/x) - \pi \cos(\pi/x)) \geq 0$$

if and only if $x \sin(\pi/x) - \pi \cos(\pi/x) \geq 0$, which is equivalent to $\tan(\pi/x) \geq \pi/x$. The latter holds true since $\tan(\theta) \geq \theta$ for $\theta \in [0, \pi/2]$. \square

The next lemma has been used in the proof of Theorem 4.5.

Lemma A.1. $P_m''(0) = T_m(v_0)T_m''(v_0)/T_m'(v_0)^2$ is increasing for $v_0 \geq 1$.

Proof. For $v_0 \geq 1$ we have the relation $T_m(v_0) = \cosh(m \operatorname{arccosh}(v_0))$. Let $\theta(v_0) = \operatorname{arccosh}(v_0)$, it holds

$$\frac{T_m(v_0)T_m''(v_0)}{T_m'(v_0)^2} = \coth(m\theta)(\coth(m\theta) - \frac{1}{m} \coth(\theta)) = c(\theta).$$

Since $\theta(v_0)$ is increasing for $v_0 \geq 1$, if $c(\theta)$ is increasing for $\theta \geq 0$ then $T_m(v_0)T_m''(v_0)/T_m'(v_0)^2$ is increasing for $v_0 \geq 1$. We have

$$c'(\theta) \geq 0 \quad \Longleftrightarrow \quad \tanh(\theta) \tanh(m\theta) - 2m \tanh(\theta)^2 + \frac{1}{m} \frac{\sinh(m\theta)^2}{\cosh(\theta)^2} \geq 0.$$

From the convexity of $\sinh(\theta)$ we deduce $\sinh(m\theta)^2/m \geq m \sinh(\theta)^2$ and thus

$$c'(\theta) \geq 0 \quad \Longleftarrow \quad \tanh(\theta) \tanh(m\theta) - m \tanh(\theta)^2 \geq 0.$$

The latter holds true since $\tanh(\theta)$ is convex and hence $\tanh(m\theta) \geq m \tanh(\theta)$. \square

References

- [1] A. Abdulle. Fourth order Chebyshev methods with recurrence relation. *SIAM Journal on Scientific Computing*, 23(6):2041–2054, 2002.
- [2] A. Abdulle and A. A. Medovikov. Second order Chebyshev methods based on orthogonal polynomials. *Numerische Mathematik*, 18:1–18, 2001.
- [3] A. Abdulle and G. A. Pavliotis. Numerical methods for stochastic partial differential equations with multiple scales. *Journal of Computational Physics*, 231(6):2482–2497, 2012.
- [4] A. Abdulle and G. Rosilho de Souza. Explicit stabilized multirate method for stiff stochastic differential equations. *Technical Report, EPFL*, 2020, arXiv:2010.15193 [math.NA].
- [5] A. Abdulle and G. Rosilho de Souza. Instabilities and order reduction phenomenon of an interpolation based multirate Runge–Kutta–Chebyshev method. *Technical Report, EPFL*, 2020, arXiv:2003.03154 [math.NA].
- [6] A. Abdulle and G. Vilmart. PIROCK: A swiss-knife partitioned implicit-explicit orthogonal Runge–Kutta Chebyshev integrator for stiff diffusion-advection-reaction problems with or without noise. *Journal of Computational Physics*, 242:869–888, 2013.

- [7] J. F. Andrus. Numerical solution of systems of ordinary differential equations into subsystems. *SIAM Journal on Numerical Analysis*, 16(4):605–611, 1979.
- [8] M. J. Berger and J. Oliger. Adaptive mesh refinement for hyperbolic partial differential equations. *Journal of Computational Physics*, 53(3):484–512, 1984.
- [9] C. N. Dawson, D. Qiang, and T. F. Dupont. A finite difference domain decomposition algorithm for numerical solution of the heat equation. *Mathematics of computation*, 57(195):63–71, 1991.
- [10] D. A. Di Pietro and A. Ern. *Mathematical aspects of discontinuous Galerkin methods*, volume 69 of *Mathématiques et Applications*. Springer, Berlin and Heidelberg, 2012.
- [11] T. Dumont, M. Duarte, S. Descombes, M. A. Dronne, M. Massot, and V. Louvet. Simulation of human ischemic stroke in realistic 3D geometry. *Communications in Nonlinear Science and Numerical Simulation*, 18(6):1539–1557, 2013.
- [12] W. E. Analysis of the heterogeneous multiscale method for ordinary differential equations. *Communications in Mathematical Sciences*, 1(3):423–436, 2003.
- [13] B. Engquist and Y. Tsai. Heterogeneous multiscale methods for stiff ordinary differential equations. *Mathematics of Computation*, 74(252):1707–1743, 2005.
- [14] C. Engstler and C. Lubich. Multirate extrapolation methods for differential equations with different time scales. *Computing*, 58(2):173–185, 1997.
- [15] W. H. Enright, T. E. Hull, and B. Lindberg. Comparing numerical methods for stiff systems of O.D.E.s. *BIT Numerical Mathematics*, 15(1):10–48, 1975.
- [16] R. E. Ewing, R. D. Lazarov, and A. Vassilev. Finite difference scheme for parabolic problems on composite grids with refinement in time and space. *SIAM Journal on Numerical Analysis*, 31(6):1605–1622, 1994.
- [17] R. E. Ewing, R. D. Lazarov, and P. S. Vassilevski. Finite difference schemes on grids with local refinement in time and space for parabolic problems I. Derivation, stability, and error analysis. *Computing*, 45(3):193–215, 1990.
- [18] M. J. Gander and L. Halpern. Techniques for locally adaptive time stepping developed over the last two decades. *Lecture Notes in Computational Science and Engineering*, 91(1):377–385, 2013.
- [19] C. W. Gear, G. Ioannis, and G. Kevrekidis. Projective methods for stiff differential equations: problems with gaps in their eigenvalue spectrum. *SIAM Journal on Scientific Computing*, 24(4):1091–1106, 2003.
- [20] C. W. Gear and D. R. Wells. Multirate linear multistep methods. *BIT Numerical Mathematics*, 24(4):484–502, 1984.
- [21] M. J. Grote, M. Mehlin, and T. Mitkova. Runge–Kutta-based explicit local time-stepping methods for wave propagation. *SIAM Journal on Scientific Computing*, 37(2):A747–A775, 2015.
- [22] G. Guennebaud and B. Jacob. Eigen v3, 2010. URL <http://eigen.tuxfamily.org/>.
- [23] A. Guillou and B. Lago. Domaine de stabilité associé aux formules d’intégration numérique d’équations différentielles, à pas séparés et à pas liés. Recherche de formules à grand rayon de stabilité. In *1er Congr. Ass. Fran. Calcul., AFCAL*, pages 43–56, Grenoble, 1960.
- [24] M. Günther, A. Kværnø, and P. Rentrop. Multirate partitioned Runge–Kutta methods. *BIT Numerical Mathematics*, 41(3):504–514, 2001.

- [25] M. Günther and P. Rentrop. Multirate ROW methods and latency of electric circuits. *Applied Numerical Mathematics*, 13(1-3):83–102, 1993.
- [26] M. Günther and A. Sandu. Multirate generalized additive Runge Kutta methods. *Numerische Mathematik*, 133(3):497–524, 2016.
- [27] E. Hairer, C. Lubich, and G. Wanner. *Geometric numerical integration*, volume 31 of *Springer Series in Computational Mathematics*. Springer, Heidelberg, 2006.
- [28] E. Hairer, S. P. Nørsett, and G. Wanner. *Solving ordinary differential equations I*, volume 8 of *Springer Series in Computational Mathematics*. Springer-Verlag, Berlin, 2008.
- [29] E. Hairer and G. Wanner. *Solving ordinary differential equations II*, volume 14 of *Springer Series in Computational Mathematics*. Springer-Verlag, Berlin, 2002.
- [30] M. Hochbruck and C. Lubich. A Gautschi-type method for oscillatory second-order differential equations. *Numerische Mathematik*, 83:403–426, 1999.
- [31] M. Hochbruck and A. Ostermann. Exponential integrators. *Acta Numerica*, 19:209–286, 2010.
- [32] E. Hofer. A partially implicit method for large stiff systems of ODEs with only few equations introducing small time-constants. *SIAM Journal on Numerical Analysis*, 13(5):645–663, 1976.
- [33] B. S. Kirk, J. W. Peterson, R. H. Stogner, and G. F. Carey. libMesh : a C++ library for parallel adaptive mesh refinement/coarsening simulations. *Engineering with Computers*, 22(3-4):237–254, 2006.
- [34] O. Knuth and R. Wolke. Implicit-explicit Runge-Kutta methods for computing atmospheric reactive flows. *Applied Numerical Mathematics*, 28(2-4):327–341, 1998.
- [35] A. Kværnø. Stability of multirate Runge-Kutta schemes. In *Proc. of the 10th Coll. on Differential Equations*, volume 1A, pages 97–105, 1999.
- [36] V. I. Lebedev. How to solve stiff systems of differential equations by explicit methods. In *Numerical methods and applications*, pages 45–80. CRC, Boca Raton, FL, 1994.
- [37] V. I. Lebedev and A. A. Medovikov. Explicit methods of second order for the solution of stiff systems of ODEs. *Russian Academy of Science*, 1994.
- [38] B. Lindberg. IMPEX: a program package for solution of systems of stiff differential equations. Technical report, Dept. of Information Processing, Royal Inst. of Tech., Stockholm, 1972.
- [39] A. A. Medovikov. High order explicit methods for parabolic equations. *BIT Numerical Mathematics*, 38(2):372–390, 1998.
- [40] R. Minero, M. J. H. Anthonissen, and R. M. M. Mattheij. A local defect correction technique for time-dependent problems. *Numerical Methods for Partial Differential Equations*, 22(1):128–144, 2006.
- [41] T. Mirzakhani. *Multi-rate Runge-Kutta-Chebyshev time stepping for parabolic equations on adaptively refined meshes*. Master thesis, Boise State University, 2017. doi:10.18122/B2V715.
- [42] J. R. Rice. Split Runge-Kutta method for simultaneous equations. *Journal of research, National Bureau of Standards. Section B, Mathematics and mathematical physics*, 64B(3):151–170, 1960.
- [43] S. Roberts, J. Loffeld, A. Sarshar, C. S. Woodward, and A. Sandu. Implicit multirate GARK methods. *Journal of Scientific Computing*, 87(4), 2021. doi:10.1007/s10915-020-01400-z.
- [44] S. Roberts, A. Sarshar, and A. Sandu. Coupled Multirate Infinitesimal GARK Schemes for Stiff Systems with Multiple Scales. *SIAM Journal on Scientific Computing*, 42(3):A1609–A1638, 2020.

- [45] G. Rosilho De Souza. *Numerical methods for deterministic and stochastic differential equations with multiple scales and high contrasts*. PhD thesis, EPFL, Lausanne, 2020. doi:10.5075/epfl-thesis-7445.
- [46] A. Sandu. A class of multirate infinitesimal GARK methods. *SIAM Journal on Numerical Analysis*, 57(5):2300–2327, 2019.
- [47] A. Sandu and M. Günther. A generalized-structure approach to additive Runge-Kutta methods. *SIAM Journal on Numerical Analysis*, 53(1):17–42, 2015.
- [48] A. Sarshar, S. Roberts, and A. Sandu. Design of high-order decoupled multirate GARK schemes. *SIAM Journal on Scientific Computing*, 41(2):A816–A847, 2019.
- [49] V. Savcenco, W. Hundsdorfer, and J. Verwer. A multirate time stepping strategy for stiff ordinary differential equations. *BIT Numerical Mathematics*, 47(1):137–155, 2007.
- [50] V. Savcenco and R. M. M. Mattheij. Multirate numerical integration for stiff ODEs. In *Progress in industrial mathematics at ECMI 2008*, volume 15, pages 327–332. Springer, Heidelberg, 2010.
- [51] J. M. Sexton and D. R. Reynolds. Relaxed Multirate Infinitesimal Step Methods for Initial-Value Problems. *Preprint*, 2019, arXiv:1808.03718 [math.NA].
- [52] G. I. Shishkin and P. N. Vabishchevich. Interpolation finite difference schemes on grids locally refined in time. *Computer Methods in Applied Mechanics and Engineering*, 190(8-10):889–901, 2000.
- [53] S. Skelboe and P. U. Andersen. Stability properties of backward Euler multirate formulas. *SIAM Journal on Scientific and Statistical Computing*, 10(5):1000–1009, 1989.
- [54] B. P. Sommeijer, L. Shampine, and J. G. Verwer. RKC: An explicit solver for parabolic PDEs. *Journal of Computational and Applied Mathematics*, 88(2):315–326, 1998.
- [55] R. Trompert and J. Verwer. A static-regridding method for two-dimensional parabolic partial differential equations. *Applied Numerical Mathematics*, 8(1):65–90, 1991.
- [56] R. Trompert and J. Verwer. Analysis of local uniform grid refinement. *Applied Numerical Mathematics*, 13(1-3):251–270, 1993.
- [57] R. Trompert and J. Verwer. Analysis of the implicit Euler local uniform grid refinement method. *SIAM Journal on Scientific Computing*, 14(2):259–278, 1993.
- [58] R. Trompert and J. Verwer. Runge–Kutta methods and local uniform grid refinement. *Mathematics of Computation*, 60(202):591–616, 1993.
- [59] P. J. Van der Houwen and B. P. Sommeijer. On the internal stability of explicit, m -stage Runge–Kutta methods for large m -values. *Zeitschrift für Angewandte Mathematik und Mechanik*, 60(10):479–485, 1980.
- [60] E. Vanden-Eijnden. Numerical techniques for multi-scale dynamical systems with stochastic effects. *Communications in Mathematical Sciences*, 1(2):385–391, 2003.
- [61] A. S. Vasudeva Murthy and J. G. Verwer. Solving parabolic integro-differential equations by an explicit integration method. *Journal of Computational and Applied Mathematics*, 39(1):121–132, 1992.
- [62] J. G. Verwer. An implementation of a class of stabilized explicit methods for the time integration of parabolic equations. *ACM Transactions on Mathematical Software (TOMS)*, 6(2):188–205, 1980.
- [63] J. G. Verwer. Explicit Runge–Kutta methods for parabolic partial differential equations. *Applied Numerical Mathematics*, 22(1-3):359–379, 1996.

- [64] J. G. Verwer, W. Hundsdorfer, and B. P. Sommeijer. Convergence properties of the Runge–Kutta–Chebyshev method. *Numerische Mathematik*, 57(1):157–178, 1990.
- [65] J. Wensch, O. Knöth, and A. Galant. Multirate infinitesimal step methods for atmospheric flow simulation. *BIT Numerical Mathematics*, 49(2):449–473, 2009.
- [66] C. J. Zbinden. Partitioned Runge-Kutta-Chebyshev methods for diffusion-advection-reaction problems. *SIAM Journal on Scientific Computing*, 33(4):1707–1725, 2011.